

---

# MambaMixer: Efficient Selective State Space Models with Dual Token and Channel Selection

---

**Ali Behrouz**  
Cornell University  
ab2947@cornell.edu

**Michele Santacatterina**  
NYU Grossman School of Medicine  
santam13@nyu.edu

**Ramin Zabih**  
Cornell University  
rdz@cs.cornell.edu

## Abstract

Recent advances in deep learning have mainly relied on Transformers due to their data dependency and ability to learn at scale. The attention module in these architectures, however, exhibits quadratic time and space in input size, limiting their scalability for long-sequence modeling. Recently, State Space Models (SSMs), and more specifically Selective SSMs (S6), with efficient hardware-aware implementation, have shown promising potential for long causal sequence modeling. They, however, use separate blocks for each channel and fail to filter irrelevant channels and capture inter-channel dependencies. Natural attempt to mix information across channels using MLP, attention, or SSMs results in further instability in the training of SSMs for large networks and/or nearly double the number of parameters. We present the MambaMixer block, a new SSM-based architecture with data-dependent weights that uses a dual selection mechanism across tokens and channels—called Selective Token and Channel Mixer. To mitigate doubling the number of parameters, we present a new non-causal heuristic of the S6 block using quasi-separable kernels with a hardware-friendly implementation that is nearly  $\times 1.8$  faster than its original implementation. Using this formulation, we further present an efficient variant of MambaMixer, called QSMixer, that mixes information along both sequence and embedding dimensions. As a proof of concept, we design Vision MambaMixer (ViM2) and Vision QSMixer (ViQS) architectures. To enhance their ability to capture spatial information in images, we present the Switch of Scans (SoS) that dynamically uses a set of useful image scans to traverse image patches. They further use a gating mechanism that employs a stack of multi-resolution convolutions to enhance the multi-resolution receptive fields. We evaluate the performance of our methods in image classification, segmentation, and object detection. Our results underline the importance of selectively mixing across both tokens and channels and show the competitive (resp. superior) performance of our methods with well-established vision (resp. SSM-based) models.

## 1 Introduction

In recent years, Transformers [1] have been the pivotal backbone architecture behind deep learning’s success, enabling a number of breakthrough advances in language modeling [2], vision [3], time series [4], healthcare [5], and several other domains [6, 7]. The attention modules in Transformers are crucial for their data dependency and enable them to generalize to unseen data and tasks given the context as input. They, however, are difficult to scale efficiently to long sequences due to their quadratic time and space complexity. Breaking this quadratic computational cost is a key step towards new possibilities for deep learning such as long-range context learning [8], large object detection [9], and long-range time series forecasting [10].

To mitigate the complexity of Transformers, several recent studies have focused on designing alternative sequence models. MLP-Mixer [11], ConvMixer [12], and MonarchMixer (M2) [13] are

motivated as simpler alternatives to attention modules by repeatedly mixing information along the sequence and model dimension axes. Efficient attentions [14–17] aim to sparsify or approximate the full attention matrix. These methods, however, either ① are based on data-independent parameters, ② introduce a trade-off between expressivity and speed, underperforming relative to Transformers when are scalable and efficient, or ③ are actually slow in practice, due to low hardware utilization [18, 17].

Recently, structured State Space Models (SSMs) have emerged as a promising class of architectures for sequence modeling [19–22]. Time-invariant (i.e., data-independent) SSMs can be viewed in both recurrent and convolution forms, making them very efficient in training (as a convolution) and inference (as a recurrent model) [23]. Despite their efficiency, their data-independent parameters limit their effectiveness in compressing context into a smaller state [8]. To alleviate this limitation, recently, Gu and Dao [8] present selective SSMs (S6) that effectively selects relevant context by making the SSM weights time variant (i.e., data dependent). Surprisingly, these SSM-based methods independently apply the SSM block to each channel, overlooking information flow across channels (also known as *Channel Mixing*). The lack of channel mixing in SSMs not only results in stability issues while scaling to large-sized networks [24], but it also causes missing the relationships among feature maps, limiting their ability to model global information in multi-dimensional data such as images, videos, and multivariate time series. Using additional channel mixing modules, however, might be challenging in large-scale networks as ① simple MLP further causes instability in the training of SSMs, resulting in poor performance [24] (See Section 4), ② effective channel mixing need to be data-dependent as some channels might be filtered for some tokens, and ③ additional data-dependent SSM or attention modules across channels result in significantly larger number of parameters ( $\approx \times 2$ ), limiting large-scale training and efficient memory usage.

We present MambaMixer, an efficient selective state space models with dual selection across both channels and tokens. MambaMixer sequentially uses *Selective Token Mixer* and *Selective Channel Mixer* blocks to mix information along the sequence and model dimension axes. Selective token mixer, which can be seen as the generalization of Mamba (see Remark 1), uses a 1D convolutions followed by a S6 block and gated it with multi-resolution convolutions to enhance the multi-resolution receptive field. To overcome the challenges of data-dependent channel mixing, we present a heuristic for bidirectional S6 using quasi-separable matrices. Compared to its naive representation, this formulation not only save about  $\times 0.5$  of parameters, but it also take advantage of a hardware-friendly and parallelizable implementation, resulting in faster training. To further improve efficiency, we present a variant of MambaMixer, called **Quasi-Separable Mixer (QSMixer)**, with hardware-friendly and parallelizable implementation. To the best of our knowledge, QSMixer is the first large-scale model that shows the power of quasi-separable matrices in sequence modeling. The design of QSMixer and MambaMixer allow them to efficiently select and mix (resp. filter) informative (resp. irrelevant) tokens and channels.

As a proof of concept, we employ MambaMixer and QSMixer blocks to design **Vision MambaMixer (ViM2)** and **ViQS** models for vision tasks. Due to the one-dimensional design of SSMs, it is challenging for a single scanning process (order of image patches) to simultaneously capture the spatial dependency across both vertical and horizontal directions, resulting in restricted receptive fields. Furthermore, while empirically using different image scanning methods [25] can help better capture the 2-dimensional spatial dependencies in images, increasing the number of scans significantly increases the number of parameters. To this end, to improve the efficiency, we present **Switch of Scans (SoS)** modules that using a router, chooses a set of effective scans for each image. To take advantage of special traits of images, ViM2 (ViQS) modifies the MambaMixer (QSMixer) block and replaces the convolutions with a stack of depth-wise convolutions that can better capture image features, enhancing global receptive fields. Our extensive experiments on ImageNet classification, object detection, and semantic segmentation tasks shows that ViM2 and ViQS achieve competitive performance with well-established vision models, and outperforms SSM-based vision models, while using less computational resources.

In the appendix, we further evaluate the performance of MambaMixer and QSMixer in time series forecasting, video understanding, and speech separation tasks. To support the architecture design of QSMixer and MambaMixer, we also report their performance without the abovementioned modifications for vision tasks (i.e., using depth-wise convolutions).

## 2 Methods: MambaMixer and QSMixer

**Preliminaries.** SSMs are known as linear time-invariant systems that map input sequence  $x(t) \in \mathbb{R}^L$  to response sequence  $y(t) \in \mathbb{R}^L$  [26]. To this end, SSMs use a latent state  $h(t) \in \mathbb{R}^{N \times L}$ , parameter  $\mathbf{A} \in \mathbb{R}^{N \times N}$ , and projection parameters  $\mathbf{B} \in \mathbb{R}^{N \times 1}$ ,  $\mathbf{C} \in \mathbb{R}^{1 \times N}$  such that:

$$h'(t) = \mathbf{A} h(t) + \mathbf{B} x(t), \quad y(t) = \mathbf{C} h(t). \quad (1)$$

To adapt these models to deep learning settings, discrete space state models [23, 27] suggests discretizing the above system using a parameter  $\Delta$  and zero-order hold, i.e.,

$$h_t = \bar{\mathbf{A}} h_{t-1} + \bar{\mathbf{B}} x_t, \quad y_t = \mathbf{C} h_t, \quad (2)$$

where  $\bar{\mathbf{A}} = \exp(\Delta \mathbf{A})$  and  $\bar{\mathbf{B}} = (\Delta \mathbf{A})^{-1} (\exp(\Delta \mathbf{A}) - I) \cdot \Delta \mathbf{B}$ .

Discrete SSMs have a convolution form and so are efficient in training. They, however, are based on data-independent parameters, meaning that parameters  $\bar{\mathbf{A}}$ ,  $\bar{\mathbf{B}}$ , and  $\mathbf{C}$  are time invariant and are the same for any input, limiting their effectiveness in compressing context into a smaller state [8]. To alleviate this limitation, recently, Gu and Dao [8] present Mamba, a selective SSMs (S6) that effectively selects relevant context by enabling dependence of the parameters  $\bar{\mathbf{B}}$ ,  $\bar{\mathbf{C}}$ , and  $\Delta$  on the input  $x_t$ , i.e.:  $\bar{\mathbf{B}}_t = \text{Linear}_{\mathbf{B}}(x_t)$ ,  $\bar{\mathbf{C}}_t = \text{Linear}_{\mathbf{C}}(x_t)$ , and  $\Delta_t = \text{Softplus}(\text{Linear}_{\Delta}(x_t))$ , where  $\text{Linear}(\cdot)$  is a linear projection and  $\text{Softplus}(\cdot) = \log(1 + \exp(\cdot))$ . This data dependency comes at the cost of the model not being able to be trained as a convolution, causing challenges for the model efficiency and scalability. To overcome this challenge, Gu and Dao [8] show that the linear recurrence in Equation 2 can be formulated as an associative scan [28], which accepts efficient parallel algorithms.

### 2.1 MambaMixer Architecture

**Selective Token Mixer.** The selective token mixer block is responsible for sequence mixing, i.e., fusing information along the sequence dimension. As the neural architecture design, we take inspiration from Mamba [8] and use a 1D convolution after the projection of input and before the S6 block. Selective token mixer, however, uses a stack of  $T$  multi-resolution convolutions with kernel size of  $k_1, \dots, k_T$  and gate it with the output of the S6 block. Not only this design provides a more generalized form and more expressive representation (see Remark 1), but it also allows the model to focus more or filter information at different levels of resolution, which is particularly important in vision and time series forecasting tasks. That is: ( $\text{Conv}(\cdot)$  is a convolution and  $\otimes$  is non-linearity.)

$$\bar{\mathbf{x}} = \sigma(\text{Conv}(\text{Linear}(x))), \quad \bar{\mathbf{x}}_{\text{Gate}} = \text{Linear}\left(\left\|_{i=1}^T \text{Conv}_{k_i}(x)\right.\right), \quad (3)$$

$$\Delta_x = \text{Softplus}(\text{Linear}_{\Delta}(x)), \quad \bar{\mathbf{C}}_x = \text{Linear}_{\mathbf{C}}(x), \quad \bar{\mathbf{B}}_x = \text{Linear}_{\mathbf{B}}(x), \quad (4)$$

$$\mathbf{y}_{\text{Token}} = \text{SSM}_{\bar{\mathbf{A}}, \bar{\mathbf{B}}_x, \bar{\mathbf{C}}_x, \Delta_x}(\bar{\mathbf{x}}) \otimes \bar{\mathbf{x}}_{\text{Gate}}. \quad (\text{Using Equation 2}) \quad (5)$$

**Remark 1.** Mamba [8] is a special case of Selective Token Mixer when  $T = 1$ ,  $k = 1$ , and so one kernel with size 1 is chosen. In this case, the convolution layer become a fully connected linear layer and the architecture is equivalent to Mamba.

**Selective Channel Mixer.** Similar to existing SSM-based architectures (e.g., S4 [29], S5 [20], S6 [8], etc.), we employ independent SSMs for each channel in the sequence mixing phase. However, in multi-dimensional data like images, videos, and time series, the inter-dependency of channels plays an important role [11, 30–32]. Channel mixing using a simple MLP block or a Gated Linear Unit (GLU) [33] are popular choices in recent models [11, 34]. They, however, result instability in the training of large SSM-based networks [24] (see Section 4). Furthermore, these blocks are data-independent, resulting in less expressive power when the channel mixer block should selectively filter irrelevant features for some tokens. To this end, we present a simple idea of using SSMs as channel mixing blocks. Accordingly, a S6 block can selectively filter irrelevant channels for each token and fuse information along the model dimension axis. In our experiments, we learned that selective channel mixing is more effective when the token mixer uses large state dimension,  $N$ , and the channel mixing is non-causal. However, increasing  $N$  and using two forward and backward SSMs can increase the number of parameters, affecting the efficiency and computational cost. Next, we take inspiration from the alternative representation of causal SSMs [35] and quasi-separable kernels

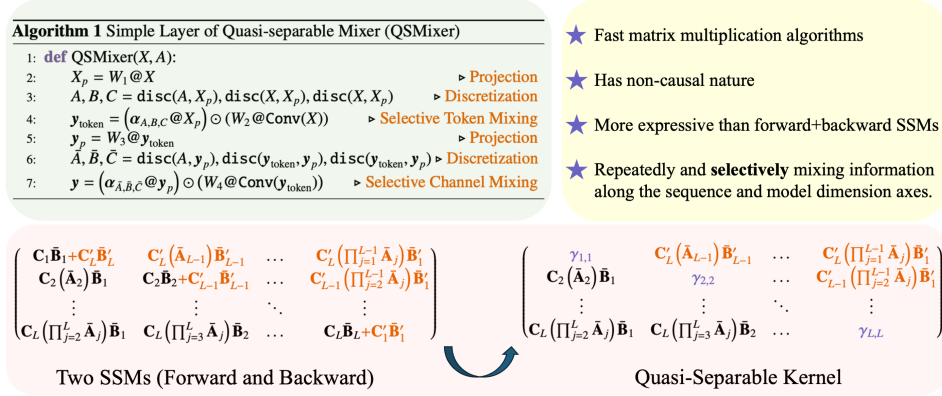


Figure 1: **Overview of the QSMixer.** QSMixer consists of mixing along both sequence and embedding dimensions using quasi-separable matrices. These matrices are a heuristic for traditional forward+backward SSMs with more representational power. They also have efficient (linear-time) matrix-vector multiplications, resulting in a very efficient training.

of HIPPO [36], and present a re-formulation of the *non-causal* selective channel mixer with more representational power, less parameters, and a more efficient (linear-time) training.

**Efficient and Effective Heuristic for Selective Channel Mixer.** Inspired by Ali et al. [35], we can recursively calculate the output of S6 as:

$$h_1 = \bar{\mathbf{B}}_1 x_1, \quad y_1 = \bar{\mathbf{C}}_1 \bar{\mathbf{B}}_1 x_1, \quad (6)$$

$$h_2 = \bar{\mathbf{A}}_2 \bar{\mathbf{B}}_1 x_1 + \bar{\mathbf{B}}_2 x_2, \quad y_2 = \bar{\mathbf{C}}_2 \bar{\mathbf{A}}_2 \bar{\mathbf{B}}_1 x_1 + \bar{\mathbf{C}}_2 \bar{\mathbf{B}}_2 x_2, \quad (7)$$

and in general case  $h_t = \sum_{i=1}^t \left( \prod_{j=i+1}^t \bar{\mathbf{A}}_j \right) \bar{\mathbf{B}}_i x_i$  and so  $y_t = \bar{\mathbf{C}}_t \sum_{i=1}^t \left( \prod_{j=i+1}^t \bar{\mathbf{A}}_j \right) \bar{\mathbf{B}}_i x_i$ . Therefore, one can reframe the formulation of S6 as  $y_f = \alpha_f x$ ,

where  $\alpha_f^{t,k} = \bar{\mathbf{C}}_t \left( \prod_{j=k+1}^t \bar{\mathbf{A}}_j \right) \bar{\mathbf{B}}_k$ . Given this formulation,  $\alpha_{t,k}$  represents the influence of  $x_k$  on  $y_f$ . Following previous studies one can represent the final output as the summation of forward and backward scans [9, 37, 38]. Writing the same formulation for the backward pass, the final output is:

$$y = y_f + y_b = (\alpha_f + \alpha_b) x = \begin{pmatrix} \alpha_f^{1,1} + \alpha_b^{L,L} & \alpha_b^{L,L-1} & \alpha_b^{L,L-2} & \dots & \alpha_b^{L,1} \\ \alpha_f^{2,1} & \alpha_f^{2,2} + \alpha_b^{L-1,L-1} & \alpha_b^{L-1,L-2} & \dots & \alpha_b^{L-1,1} \\ \alpha_f^{3,1} & \alpha_f^{3,2} & \alpha_f^{3,3} + \alpha_b^{L-3,L-3} & \dots & \alpha_b^{L-2,1} \\ \vdots & \vdots & \vdots & \ddots & \vdots \\ \alpha_f^{L,1} & \alpha_f^{L,2} & \alpha_f^{L,3} & \dots & \alpha_f^{L,L} + \alpha_b^{1,1} \end{pmatrix} \begin{pmatrix} x_1 \\ x_2 \\ x_3 \\ \vdots \\ x_L \end{pmatrix}, \quad (8)$$

where  $\alpha_f^{t,k} = \bar{\mathbf{C}}_t \left( \prod_{j=k+1}^t \bar{\mathbf{A}}_j \right) \bar{\mathbf{B}}_k$  and  $\alpha_b^{t,k} = \bar{\mathbf{C}}'_{L+1-t} \left( \prod_{j=L-k}^{L-t+1} \bar{\mathbf{A}}'_j \right) \bar{\mathbf{B}}'_{L+1-k}$ . Surprisingly, using a small modification: i.e., making the diagonal elements scalar, see Fig. 1; the above matrix is in the form of quasi-separable matrices (see Appendix A for the background of these matrices). Accordingly, we replace the diagonal elements with scalar  $\gamma_1, \dots, \gamma_L$  and re-formulate the bidirectional S6 as a matrix multiplication of quasi-separable matrices. Interestingly, quasi-separable matrices are theoretically well-known and have efficient (linear-time) matrix-vector multiplication [39, 40], resulting in linear time training of selective channel mixer module. Furthermore, while in Eq. 8 the diagonal elements are tied to the other elements by  $\mathbf{C}_i$ s and  $\bar{\mathbf{B}}_j$ s, the modified formulation provides more representation power and so is more expressive. Also, due to the nature of this formulation, there is no need to use separate projections, convolutions, etc. for forward and backward scans as in existing non-causal methods [9, 37, 38], resulting in significant parameter decrease. In our implementation of selective channel mixer inspired by Pernet [40], we decompose the quasi-separable matrix into its upper, lower and diagonal terms and perform multiplication in parallel (See Appendix D).

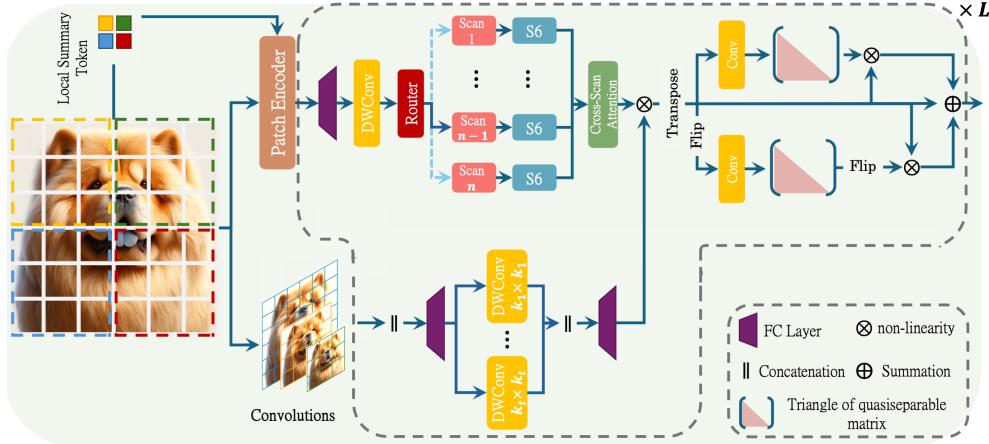


Figure 2: **Architecture design and overview of the ViM2.** ViM2 consists of two branches of multi-resolution convolutions and a sequence encoder, followed by a selective channel mixer. This combination allows the model to capture local, long-range, and inter-channel dependencies.

## 2.2 QSMixer: An Efficient Architecture using Quasi-Separable Matrices

The above re-formulation brings an interesting connection between the MambaMixer and a class of machine learning models that operate by repeatedly mixing information using a single operator (e.g., matrix multiplication or convolution) along the sequence and model dimension axes: e.g., Monarch Mixer (M2) [13], MLP-Mixer [11], and ConvMixer [12]. Taking inspiration from these work and the above re-formulation, we further simplify the MambaMixer block, use a scalar matrix as  $A$ , and use the above heuristic for *both* selective token and channel mixing. Accordingly, the resulted architecture, called **Quasi-Separable Mixer (QSMixer)**, uses quasi-separable matrices gated with a linear (or multi-resolution convolution) layer(s) as the operator for repeatedly mixing information along the sequence and model dimension axes (pseudocode in Fig. 1). A simple formulation is as follows:

$$\tilde{\mathbf{Y}} = Q_{\tilde{A}, \tilde{B}, \tilde{C}}^{(1)} X \otimes \left( W_1 \text{Conv} \left( \left\| \left\|_{i=1}^T \text{Conv}_{k_i}(X) \right\| \right\| \right) \right) \quad (9)$$

$$\mathbf{Y}^T = Q_{A', B', C'}^{(2)} \tilde{\mathbf{Y}}^T \otimes (W_2 \tilde{\mathbf{Y}}^T), \quad (10)$$

where  $W_1$  and  $W_2$  are learnable parameters and  $\otimes$  is gating with non-linearity. Note that while the multiplication of dense matrices are based on general matrix multiplication algorithms (GEMM), the multiplication of quasi-separable matrices are based on their more efficient algorithms [39, 40], which we show that it can be parallelized to fully take advantage of the GPU (See Appendix D). Compared to the existing architectures in the abovementioned class of models, QSMixer uses data-dependent weights for both token and channel mixing operations and so is capable of selectively filter irrelevant information for each token. On the other hand, MLP-Mixer, ConvMixer, and an M2 block use data-independent weights, limiting their ability to select informative context.

Inspired by Liu et al. [41], in the next theorem we connect QSMixer and dual-attentions (spatial and channel attentions); e.g., DaViT [42], DANet [43]. The proof is provided in Appendix C.

**Theorem 1.** *Replacing  $\text{Softmax}(\cdot)$  with a linear kernel [44] in dual attentions [42, 43] results in a model that is a special case of MambaMixer and so QSMixer.*

## 3 Vision MamabMixer (ViM2) and Vision QSMixer (ViQS)

In this section, as a proof of concept, we use MambaMixer and QSMixer blocks for vision tasks. In Appendix H, we further extend them to time series, video, and speech data.

The main challenge to employ sequence encoders for vision tasks is their limited ability to simultaneously capture the spatial dependency across both vertical and horizontal directions, resulting in restricted receptive fields. To this end, several studies suggest using different scanning (order of image patches). However, surprisingly, it is not studied that how different scanning can address this issue

and provide additional inductive bias. Furthermore, using different scans comes with considerable increase in the number of parameters and inefficiency in training as it requires employing independent SSMs for each scans. To this end, we present Switch of Scans (SoS) to improve the effectiveness and efficiency of using different scannings.

**Patching.** Given a 2D image  $I \in \mathbb{R}^{H \times W \times C}$ , we transform it into a flattened 2D patches  $I_p \in \mathbb{R}^{K \times (P^2 \times C)}$ , where  $(H, W)$  is the image size,  $C$  is the #channels, and  $P$  is the patch size. We then linearly project patches each of which into a vector with size  $D$  and further add positional encoding  $E_{\text{pos}} \in \mathbb{R}^{(K+1) \times D}$ . The additional token for each image is the class token that is also used by ViT [3] and ViM [9].

**Switch of Scans (SoS).** As discussed earlier, while using different scans improves the performance, it comes with a considerable increase in the #FLOPs. To overcome this trade-off, inspired by mixture of expert techniques [45, 46], we present SoS that dynamically select the best set of scans for each image using a router. In our experiments, we observe that high-level features are more important when deciding on which scans are more useful. As an example, in image classification task, if the object is closed to upper-left, a scan from bottom-right toward upper-left is more effective. To this end, we use  $\ell^2$  local windows with size  $\frac{W}{\ell} \times \frac{H}{\ell}$  (usually  $\ell^2 = 4$  or 9) and summarize the information in each of them into a Local Summary Token (LST)  $S_i$  for  $i = 1, \dots, \ell^2$ . For each patch  $I_p$ , we concatenate its corresponding local summary token to its patch encoding.

Given  $n \in \mathbb{N}$ , we follow Riquelme et al. [46] and use  $G(x) = \text{Top}_n(\text{Softmax}(W_s x + b_s))$  as the router, where  $W_s$  and  $b_s$  are learnable parameters, and the output of  $\text{Top}_n(\cdot)$  is the  $k$  scans with higher probability. Accordingly, for each image, the router decides which set of the scans ( $n$  scans) are more effective. The main reason of calling this process a switch comes from our experiments that we found for classification tasks, using  $n = 1$  (i.e, top-1 scan) but bidirectional is enough to achieve a good performance while avoiding parameter increase. Finally, when  $n \geq 2$ , we use a cross-scan attention to combine the outputs of different selected scans by the router. In practice  $n \leq 10$  and this module does not add significant number of parameters. The details of the initial pool of scans are in Appendix G.

**Selective Channel and Token Mixer.** In ViM2, we use MambaMixer block and so the selective token mixer is the architecture that we introduced in Section 2.1. For the channel mixing, we use the simplified and faster version, i.e., quasi-separable formulation. In ViQS, we use QSMixer block and so both selective token and channel mixers are based on the quasi-separable formulation.

**Gating with Multi-resolution Convolutions.** We further modified the gating of the MambaMixer and QSMixer to adapt them for vision tasks. While sequence encoders like Transformers [1, 3] and SSMs [29, 47] show promising results in vision tasks, they perform poorly on dense images and dense prediction tasks, which is caused by the lack of inner-patch information flow as well as missing features at different scales. To this end, inspired by the success of Multi-Receptive Field Feature Pyramid [48], we use a set of convolutions to extract multi-resolution features from the input images. We construct features  $F_1, F_2$ , and  $F_3$  with resolution  $\frac{1}{8}, \frac{1}{16}$ , and  $\frac{1}{32}$ , concatenate them, and pass the features to a linear projection layer to construct  $C \in \mathbb{R}^{(\frac{HW}{64} + \frac{HW}{256} + \frac{HW}{1024}) \times D}$ . We use depth-wise separable convolutions with different kernel size  $k_i \times k_i$ , each of which on the features of the same resolution:

$$F_{\text{conv}} = W_{c_1} \text{DWConv} \left( W_{c_2} \left[ F_1 \parallel F_2 \parallel F_3 \right] \right), \quad (11)$$

where  $W_{c_1}$  and  $W_{c_2}$  are learnable parameters. Note that while the original QSMixer and MambaMixer blocks also uses a stack of convolutions, the main change is that instead of applying convolutions on the patched images, we use the stack of convolutions on the multi-resolution image features, without patching. Also, instead of 1D convolutions, here, we use depth-wise separable convolutions.

## 4 Experiments

We compare MambaMixer and QSMixer with Transformers, CNN-based, mixer models, and SSM-based architectures on vision tasks: i.e., image classification, object detection, semantic segmentation. We show that the proposed architectures match or outperform baselines using neither attention or MLP on the sequence axis while having less FLOPs and memory usage. Results further indicate the importance of channel mixing, more specifically selective channel mixing, in SSM-based architectures. Additional experiments on time series forecasting, video understanding, and speech separation tasks are given in Appendix H and Appendix I. Experimental details are in Appendix G.

Table 2: Accuracy comparison across various models on ImageNet-1K. Full list in Appendix I.

Method	Size	#Param. (M)	#FLOPs	Top-1	Top-5
ConvNets					
ResNet-50 [2016]	224 <sup>2</sup>	25	4.1	78.3	94.3
ResNet-101 [2016]	224 <sup>2</sup>	45	7.9	80.0	95.0
ResNet-152 [2016]	224 <sup>2</sup>	60	11.6	81.3	95.5
RegNetY-4G [2020]	224 <sup>2</sup>	21	4.0	80.0	-
RegNetY-8G [2020]	224 <sup>2</sup>	39	8.0	81.7	-
RegNetY-16G [2020]	224 <sup>2</sup>	84	16.0	82.9	-
EffNet-B3 [2019]	300 <sup>2</sup>	12	1.8	81.6	-
EffNet-B4 [2019]	380 <sup>2</sup>	19	4.2	82.9	-
RepViT-M1.5 [2024]	224 <sup>2</sup>	14.0	-	82.3	-
RepViT-M2.3 [2024]	224 <sup>2</sup>	22.9	-	83.3	-
Mixer					
Mixer-B/16 [2021]	224 <sup>2</sup>	59	-	76.4	-
Mixer-L/16 [2021]	224 <sup>2</sup>	207	-	71.8	-
ConvMixer-768/32 [2023]	224 <sup>2</sup>	21	-	80.2	-
ConvMixer-1536/20 [2023]	224 <sup>2</sup>	52	-	81.4	-
M2-ViT-b [2023]	224 <sup>2</sup>	45	-	79.5	94.5
Transformers					
ViT-b + Monarch [2023]	224 <sup>2</sup>	33	-	78.9	94.2
ViT-B/16 [2021]	384 <sup>2</sup>	86	17.6	77.9	-
DeiT-S [2021]	224 <sup>2</sup>	22	4.6	79.8	-
DeiT-B [2021]	224 <sup>2</sup>	86	17.5	81.8	-
Swin-T [2021]	224 <sup>2</sup>	29	4.5	81.3	95.5
Swin-S [2021]	224 <sup>2</sup>	50	8.7	83.0	96.2
Swin-B [2021]	224 <sup>2</sup>	88	15.4	83.5	96.5
iFormer-S [2022]	224 <sup>2</sup>	20	4.8	83.4	96.6
iFormer-B [2022]	224 <sup>2</sup>	48.0	9.4	84.6	97.0
Wave-ViT-S [2022]	224 <sup>2</sup>	22.7	4.7	83.9	96.6
Wave-ViT-B [2022]	224 <sup>2</sup>	33.5	7.2	84.8	97.1
Dual-attention					
DaViT-T [2022]	224 <sup>2</sup>	28.3	4.5	82.8	-
DaViT-S [2022]	224 <sup>2</sup>	49.7	8.8	84.2	-
DaViT-B [2022]	224 <sup>2</sup>	87.9	15.5	84.6	-

Method	Size	#Param. (M)	#FLOPs	Top-1	Top-5
Efficient Transformers					
MobileViT-S [2022]	256 <sup>2</sup>	5.6	2.0	78.4	-
EfficientFormer-L1 [2022]	224 <sup>2</sup>	12.3	1.3	79.2	-
EfficientFormer-L3 [2022]	224 <sup>2</sup>	31.3	3.9	82.4	-
EfficientFormer-L7 [2022]	224 <sup>2</sup>	82	10.2	83.3	-
EfficientMod-S [2024]	224 <sup>2</sup>	12.9	1.4	81.0	-
FastViT-T12 [2023]	256 <sup>2</sup>	6.8	1.4	79.1	-
FastViT-MA36 [2023]	256 <sup>2</sup>	42.7	7.9	83.9	-
FAT-B1 [2023]	224 <sup>2</sup>	7.8	1.2	80.1	-
FAT-B3-ST [2023]	224 <sup>2</sup>	29	4.7	83.0	-
SSMs					
S4ND-ConvNeXt-T [2022]	224 <sup>2</sup>	30	-	82.2	-
S4ND-ViT-B [2022]	224 <sup>2</sup>	89	-	80.4	-
Hyena-ViT-B [2023]	224 <sup>2</sup>	88	-	78.5	93.6
VMamba-T [2024]	224 <sup>2</sup>	22	4.9	82.2	-
VMamba-S [2024]	224 <sup>2</sup>	44	8.7	83.5	-
VMamba-B [2024]	224 <sup>2</sup>	75	15.4	83.2	-
SiMBA-S [2024]	224 <sup>2</sup>	15.3	2.4	81.7	95.9
SiMBA-S (Monarch) [2024]	224 <sup>2</sup>	18.5	3.6	81.1	-
SiMBA-B [2024]	224 <sup>2</sup>	22.8	4.2	83.5	-
SiMBA-B (Monarch) [2024]	224 <sup>2</sup>	26.9	5.5	82.6	-
SiMBA-L [2024]	224 <sup>2</sup>	40	9.0	84.4	-
SiMBA-L (Monarch) [2024]	224 <sup>2</sup>	42	8.7	83.8	-
ViM-T [2024]	224 <sup>2</sup>	7	1.5	76.1	-
LocalViM-T [2024]	224 <sup>2</sup>	8	1.5	75.8	-
ViM-S [2024]	224 <sup>2</sup>	26	5.1	80.5	-
LocalViM-S [2024]	224 <sup>2</sup>	28	4.8	81.0	-
ViM2-MLP (Baseline)	224 <sup>2</sup>	40	9.0	80.1	94.8
ViM2-T (ours)	224 <sup>2</sup>	13.2	2.1	81.9	95.9
ViQS-T (ours)	224 <sup>2</sup>	10.1	1.9	81.7	95.8
ViM2-S (ours)	224 <sup>2</sup>	28	5.3	83.8	96.6
ViQS-S (ours)	224 <sup>2</sup>	23	4.7	83.8	96.5
ViM2-B (ours)	224 <sup>2</sup>	74	17.9	85.0	97.1
ViQS-B (ours)	224 <sup>2</sup>	45	9.0	84.9	97.0
ViM2-L (ours)	224 <sup>2</sup>	122	23.2	85.5	97.3

**Models.** We follow the existing studies and use three scales of our model: i.e., Tiny, Small, and Base, referred to using the short form of T, S, B, respectively. To show the effectiveness of SoS, we also use large scale of ViM2-L. The details of these architectures are reported in Appendix G. As ablation studies, we further replace our selective channel mixer in ViM2 with MLP, called ViM2-MLP.

#### 4.1 Image Classification

**Goals and Baselines.** In this section we evaluate: ① The performance of MambaMixer and QS-Mixer as the *sequence encoder backbone* and compare them with the state-of-the-art sequence encoders [1, 23, 19, 29, 20, 8] on sequence CIFAR (sCIFAR) and ImageNet-1K [49] to show their effectiveness (see Appendix I for more experiments); ② We compare the ViM2 and ViQS with convolution-based vision models [50–53], Mixer methods [11–13], Transformer-based [13, 54–57], Dual-attention [42], efficient ViT [58–62], and SSM-based vision models [9, 24, 41, 47, 63, 64] on ImageNet-1K; ③ We evaluate the effectiveness of selective channel mixing with different sequence encoder backbones, e.g., S4 [19], Hippo [23], Mamba [8], and our selective token mixers in MambaMixer and QSMixer; ④ We perform ablation study on the components of ViQS and ViM2 to support the architecture design; and ⑤ Evaluate the effect of resolution on accuracy, FLOPs, and memory to support the scalability and generalizability of our methods.

**MambaMixer and QSMixer as Backbone.** Table 1 reports the performance of our methods and baselines. sCIFAR is a pixel-level classification task that shows the ability of the method to capture long-range dependencies. QSMixer outperforms Transformers by 29.6% (resp. 2.3%), HiPPO-RNN by 30.7%, S4 by 0.7% (resp. 2.1%), S4D by 1.9% (resp. 0.8%), S5 by 2.1% (resp. 3.3%), and Mamba by 1.7% (resp. 0.7%) on sCIFAR (resp. ImageNet-1K). MambaMixer further outperforms even QSMixer by 0.5% (resp. 0.2%) on sCIFAR (resp. ImageNet), indicating the effectiveness of both methods for capturing long-range dependencies.

Table 1: Classification on sCIFAR and ImageNet.

Method	sCIFAR	ImageNet-1K
Transformer [1]	62.2	78.9
HiPPO-RNN [23]	61.1	-
S4 [19]	91.1	79.1
S4D [29]	89.9	80.4
S5 [20]	89.7	77.9
Mamba [8]	90.1	80.5
QSMixer	91.8	81.2
MambaMixer	92.3	81.4

**ViM2 and ViQS as Vision Models.** ViM2 and ViQS exhibit superior performance in image classification, outperforming the best mixer architecture by 3.55% on average, the best efficient transformer-based by 1.2% on average, dual attention-based model by 0.7% on average, and the best SSM-based model without (resp. with) channel mixing by 1.6% (resp. 0.7%) on average. They also achieve on par performance with the very recent carefully designed convolution-based architecture (RepViT [53]) and the best transformer-based baseline, Wave-ViT [65]. It is notable that ViM2 and ViQS are based on simple but effective modifications to adapt a sequence encoder (MambaMixer or QSMixer) to vision tasks. They, however, perform better than or on par with carefully designed transformer-based and efficient transformers models in terms of #FLOPs and accuracy—even though the latter group was explicitly designed for the trade-off of efficiency and accuracy. Comparing to mixer models, the superior performance of ViQS show the power of quasi-separable matrices and the selection mechanism, data-dependency and gating, across both sequence and channels. The superior performance compared to SSM-based vision models highlights the importance of *data-dependent* channel mixing and the Switch of Scan module. For the efficiency evaluation, we further compare their throughput with baselines in Appendix I.

Table 3: The effect of selective channel mixing.

Method	#Param. (M)	Top-1	Top-5
S4	17.7	68.9	90.5
S4 + MLP	18.3	72.7	92.8
S4 + QS	18.3	73.1	92.8
Hippo	16.9	67.8	90.2
Hippo + MLP	18.5	75.3	93.5
Hippo + QS	18.5	77.5	94.0
Mamba	16.2	73.0	91.1
Mamba + MLP	17.6	79.4	94.2
Mamba + QS	17.6	80.6	95.3
ViM2 - QS	11.3	78.4	93.9
ViM2(MLP)	13.1	80.0	95.0
ViM2	13.2	81.9	95.9
ViQS - QS	9.8	78.2	94.3
ViQS(MLP)	10.1	80.3	95.1
ViQS	10.1	81.7	95.8

Table 4: Ablation on ViQS and ViM.

Method	#Param. (M)	Throughput (img/s)	Top-1 Accuracy
ViQS	10.1	1172	81.7
w/o QS	9.8	1219	78.2
w/ f+b	13.0	1007	81.6
w/o LST	10.1	1174	81.6
w/o Conv	10.1	1168	80.4
w/o SoS	10.1	1129	81.2
w/o Attn	10.1	1172	81.7
ViM2	13.2	1096	81.9
w/o QS	11.3	1148	78.4
w/ f+b	16.8	1162	81.4
w/o LST	13.2	1095	81.6
w/o Conv	13.2	1093	80.0
w/o SoS	13.2	1067	80.8
w/o Attn	13.2	1095	81.5

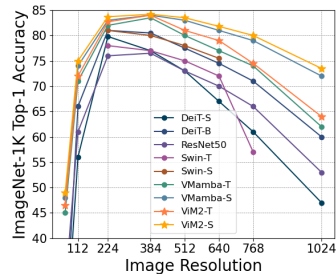


Figure 3: Input scaling.

**The Effect of Resolution on Accuracy, FLOPs, and Throughput.** Showing a good performance for high-resolution images and on images with different resolutions is challenging for most existing methods [66], as it requires capturing long-range dependencies. In this section, we evaluate the performance and efficiency of ViM2 and ViQS when are trained on  $224 \times 224$  image but are testing with images with resolutions ranging from  $384 \times 384$  to  $1024 \times 1024$ . We report the results of these models and baselines in Figure 3. ViM2 and ViQS show more robustness compared to the existing baselines, showing their ability to capture long-range dependencies. The results for FLOPs and throughput comparison are reported in Appendix I.

**The Effect of Selective Channel Mixer.** To support the importance of channel mixing and more specifically *data-dependent* channel mixing, we evaluate the performance of S4, Hippo, Mamba, and our selective token mixers with and without channel mixing on ImageNet-1K. We use MLP and our quasi-separable formulation of selective channel mixing (referred to as QS) as the channel mixing methods. Table 3 reports the results. First, results highlight the importance of channel mixing as an MLP block can significantly improve the performance of all baselines. Using selective channel mixing can further improve the importance of all baselines as it data-dependent channel selection mechanism can filter irrelevant channels for each token.

**Ablation Study.** To support the architecture choice and design of ViQS and ViM2, we perform a case study and remove a component at a time while keeping the other parts unchanged: in each block, row 1 is the complete architecture, row 2 removes the selective channel mixing, row 3 uses backward + forward implementation of bi-directional SSMs (naive implementation of selective channel mixer), row 4 removes the local summary token, row 5 removes the convolutions and instead uses a fully connected layer, row 6 removes the Switch of Scans, and row 7 replaces the cross-scan attention with summation. The results show that each of the components of these architectures contributes to its performance. More specifically, the quasi-separable formulation and our implementation of channel mixer results in near 10% throughput improvement. The more contribution comes from the channel mixing, where the lack of channel mixing results in 3.5% performance drop on average. We further discuss the effect of scans and SoS in Appendix I.



Table 5: Semantic segmentation results on ADE20K using UperNet [67]. Full list in Appendix I.

Method	Size	mIoU-S	mIoU-M	#Param. (M)	#FLOPs
ResNet-50 [2016]	512 <sup>2</sup>	42.1	42.8	67	953
ResNet-101 [2016]	512 <sup>2</sup>	42.9	44.0	85	1030
DeiT-S + MLN [2021]	512 <sup>2</sup>	43.8	45.1	58	1217
DeiT-B + MLN [2021]	512 <sup>2</sup>	45.5	47.2	144	2007
Swin-T [2021]	512 <sup>2</sup>	44.4	45.8	60	945
Swin-S [2021]	512 <sup>2</sup>	47.6	49.5	81	1039
Swin-B [2021]	512 <sup>2</sup>	48.1	49.7	121	1188
ConvNeXt-T [2022]	512 <sup>2</sup>	46.0	46.7	60	939
ConvNeXt-S [2022]	512 <sup>2</sup>	48.7	49.6	82	1027
ConvNeXt-B [2022]	512 <sup>2</sup>	49.1	49.9	122	1170
ViT-CoMer-T [2024]	512 <sup>2</sup>	43.0	44.3	38.7	-
ViT-CoMer-S [2024]	512 <sup>2</sup>	46.5	47.7	61.4	-
ViT-CoMer-B [2024]	512 <sup>2</sup>	48.8	49.4	144.7	-
ViM-T [2024]	512 <sup>2</sup>	41.0	-	13	-
ViM-S [2024]	512 <sup>2</sup>	44.9	-	46	-
SiMBA-S [2024]	512 <sup>2</sup>	49.0	49.6	62	-
VMamba-T [2024]	512 <sup>2</sup>	47.3	48.3	55	948
VMamba-S [2024]	512 <sup>2</sup>	49.5	50.5	76	1039
VMamba-B [2024]	512 <sup>2</sup>	50.0	51.3	110	1170
ViQS-T	512 <sup>2</sup>	49.6	50.1	51	918
ViM2-T	512 <sup>2</sup>	48.9	49.9	51	920
ViQS-S	512 <sup>2</sup>	49.7	50.8	68	964
ViM2-S	512 <sup>2</sup>	50.3	51.5	74	1025

Table 6: Object detection and instance segmentation results on COCO dataset. Full list in Appendix I.

Method	AP <sup>b</sup>	AP <sup>b</sup> <sub>50</sub>	AP <sup>b</sup> <sub>75</sub>	AP <sup>m</sup>	AP <sup>m</sup> <sub>50</sub>	AP <sup>m</sup> <sub>75</sub>	#Param. (M)
ResNet-50 [2016]	38.2	58.8	41.4	34.7	55.7	37.2	44
ResNet-101 [2016]	38.2	58.8	41.4	34.7	55.7	37.2	63
Swin-T [2021]	42.7	65.2	46.8	39.3	62.2	42.2	48
Swin-S [2021]	44.8	66.6	48.9	40.9	63.2	44.2	69
Swin-B [2021]	46.9	-	-	42.3	-	-	107
ViT-Adapter-S [2021]	44.7	65.8	48.3	39.9	62.5	42.8	48
ViT-Adapter-B [2021]	47.0	68.2	51.4	41.8	65.1	44.9	102
ConvNeXt-T [2022]	44.2	66.6	48.3	40.1	63.3	42.8	48
ConvNeXt-S [2022]	45.4	67.9	50.0	41.8	65.2	45.1	70
ConvNeXt-B [2022]	47.0	69.4	51.7	42.7	66.3	46.0	108
PVTv2-B2 [2022]	45.3	67.1	49.6	41.2	64.2	44.4	45
PVTv2-B3 [2022]	47.0	68.1	51.7	42.5	65.7	45.7	65
PVTv2-B5 [2022]	47.4	68.6	51.9	42.5	65.7	46.0	102
ViT-CoMer-T [2024]	42.1	62.7	45.3	38.0	60.1	40.5	29
ViT-CoMer-S [2024]	45.8	67.0	49.8	40.5	63.8	43.3	50
ViT-CoMer-B [2024]	47.6	68.9	51.9	41.8	65.9	44.9	129
SiMBA-S [2024]	46.9	68.6	51.7	42.6	65.9	45.8	60
VMamba-T [2024]	46.5	68.5	50.7	42.1	65.5	45.3	42
VMamba-S [2024]	48.2	69.7	52.5	43.0	66.6	46.4	64
VMamba-B [2024]	48.5	69.6	53.0	43.1	67.0	46.4	96
ViQS-T	47.5	69.0	50.9	42.6	65.8	45.7	40
ViM2-T	48.1	69.9	52.8	43.2	66.7	46.6	48
ViQS-S	48.2	69.8	53.0	43.3	66.9	46.7	68
ViM2-S	48.7	69.8	52.8	43.5	66.8	46.9	80

## 4.2 Other Downstream Tasks: Segmentation and Detection

We further evaluate the performance of ViM2 and ViQS on segmentation and object detection tasks to support their applicability in diverse tasks.

**Semantic Segmentation.** The results of the performance comparison of ViM2 and ViQS with baselines are reported in Table 5. Results show that with similar scale and size, ViM2 and ViQS achieve superior performance, outperforming VMamba by 0.7% (resp. 0.5%), ViT-CoMer by 3.3% (resp. 3.5%) Swin by 2.9% (resp. 2.3%), and ResNet by 6.1% (resp. 7.2%) mIoU (resp. mIoU-M) improvement on average. We attribute this superior performance to the design of MambaMixer and QSMixer, where they not only can capture long-range dependencies, but they also use multi-resolution convolutions that enhance the receptive field.

**Object Detection on COCO.** Table 6 reports the performance of ViM2, ViQS, and baselines in object detection tasks on COCO dataset [69]. The ability of MambaMixer and QSMixer blocks in capturing long-range dependencies results in the superior performance of ViM2 and ViQS as they enable them to capture large objects that other transformer-based methods fails to capture. ViQS and ViM2 achieve on par performance with VMamba-B while having almost 30% less parameters; and outperform ViT-CoMer, Swin, ViM, ViT, and ResNet.

## 5 Conclusion

In this paper, we present MambaMixer and QSMixer, two data-dependent SSM-based architectures that recursively and *selectively* mix information across sequence and model dimensions, with hardware-friendly and efficient (linear-time) training. Our formulation connects selective SSMs with mixer, dual attention, and 2-dimensional SSM-based methods, making the implementation of SSMs faster, and also bringing data-dependency to mixer architectures. We discuss the challenges of adapting SSMs to vision tasks (i.e., inefficiency because of multiple image scans and limited receptive field), and present ① Switch of Scans that dynamically finds the most effective scans for each image, and ② a gating module to enhance the receptive field using a stack of multi-resolution convolutions, resulting in designing two vision models ViM2 and ViQS that are based on MambaMixer and QSMixer. Our experiments show that ViM2 and ViQS achieve superior performance compared to SSM-based baselines and have on par performance with specialized Transformer-based architecture.

## Acknowledgments and Disclosure of Funding

This material is based upon work supported by the National Science Foundation under Grant No. 2306556.

## References

- [1] Ashish Vaswani, Noam Shazeer, Niki Parmar, Jakob Uszkoreit, Llion Jones, Aidan N Gomez, Łukasz Kaiser, and Illia Polosukhin. Attention is all you need. *Advances in neural information processing systems*, 30, 2017.
- [2] Thomas Wolf, Lysandre Debut, Victor Sanh, Julien Chaumond, Clement Delangue, Anthony Moi, Pierric Cistac, Tim Rault, Rémi Louf, Morgan Funtowicz, et al. Huggingface’s transformers: State-of-the-art natural language processing. *arXiv preprint arXiv:1910.03771*, 2019.
- [3] Alexey Dosovitskiy, Lucas Beyer, Alexander Kolesnikov, Dirk Weissenborn, Xiaohua Zhai, Thomas Unterthiner, Mostafa Dehghani, Matthias Minderer, Georg Heigold, Sylvain Gelly, Jakob Uszkoreit, and Neil Houlsby. An image is worth 16x16 words: Transformers for image recognition at scale. In *International Conference on Learning Representations*, 2021. URL <https://openreview.net/forum?id=YicbFdNTTy>.
- [4] Haoyi Zhou, Shanghang Zhang, Jieqi Peng, Shuai Zhang, Jianxin Li, Hui Xiong, and Wancai Zhang. Informer: Beyond efficient transformer for long sequence time-series forecasting. In *Proceedings of the AAAI conference on artificial intelligence*, volume 35, pages 11106–11115, 2021.
- [5] Jerry Tang, Meng Du, Vy Vo, VASUDEV LAL, and Alexander Huth. Brain encoding models based on multimodal transformers can transfer across language and vision. In A. Oh, T. Neumann, A. Globerson, K. Saenko, M. Hardt, and S. Levine, editors, *Advances in Neural Information Processing Systems*, volume 36, pages 29654–29666. Curran Associates, Inc., 2023. URL [https://proceedings.neurips.cc/paper\\_files/paper/2023/file/5ebbbac62b968254093023f1c95015d3-Paper-Conference.pdf](https://proceedings.neurips.cc/paper_files/paper/2023/file/5ebbbac62b968254093023f1c95015d3-Paper-Conference.pdf).
- [6] Alec Radford, Jong Wook Kim, Tao Xu, Greg Brockman, Christine McLeavey, and Ilya Sutskever. Robust speech recognition via large-scale weak supervision. In *International Conference on Machine Learning*, pages 28492–28518. PMLR, 2023.
- [7] Ali Behrouz, Parsa Delavari, and Farnoosh Hashemi. Unsupervised representation learning of brain activity via bridging voxel activity and functional connectivity. In *NeurIPS 2023 AI for Science Workshop*, 2023. URL <https://openreview.net/forum?id=HSVg7qFFd2>.
- [8] Albert Gu and Tri Dao. Mamba: Linear-time sequence modeling with selective state spaces. *arXiv preprint arXiv:2312.00752*, 2023.
- [9] Lianghui Zhu, Bencheng Liao, Qian Zhang, Xinlong Wang, Wenyu Liu, and Xinggang Wang. Vision mamba: Efficient visual representation learning with bidirectional state space model. *arXiv preprint arXiv:2401.09417*, 2024.
- [10] Shizhan Liu, Hang Yu, Cong Liao, Jianguo Li, Weiyao Lin, Alex X Liu, and Schahram Dustdar. Pyraformer: Low-complexity pyramidal attention for long-range time series modeling and forecasting. In *International conference on learning representations*, 2021.
- [11] Ilya O Tolstikhin, Neil Houlsby, Alexander Kolesnikov, Lucas Beyer, Xiaohua Zhai, Thomas Unterthiner, Jessica Yung, Andreas Steiner, Daniel Keysers, Jakob Uszkoreit, et al. Mlp-mixer: An all-mlp architecture for vision. *Advances in neural information processing systems*, 34: 24261–24272, 2021.
- [12] Asher Trockman and J Zico Kolter. Patches are all you need? *Transactions on Machine Learning Research*, 2023. ISSN 2835-8856. URL <https://openreview.net/forum?id=rAnB7JSMXL>. Featured Certification.
- [13] Daniel Y Fu, Simran Arora, Jessica Grogan, Isys Johnson, Sabri Eyuboglu, Armin W Thomas, Benjamin Frederick Spector, Michael Poli, Atri Rudra, and Christopher Re. Monarch mixer: A simple sub-quadratic GEMM-based architecture. In *Thirty-seventh Conference on Neural Information Processing Systems*, 2023. URL <https://openreview.net/forum?id=cB0BImqSS9>.

- [14] Guangxuan Xiao, Yuandong Tian, Beidi Chen, Song Han, and Mike Lewis. Efficient streaming language models with attention sinks. In *The Twelfth International Conference on Learning Representations*, 2024. URL <https://openreview.net/forum?id=NG7sS51zVF>.
- [15] Praneeth Kacham, Vahab Mirrokni, and Peilin Zhong. Polysketchformer: Fast transformers via sketches for polynomial kernels. *arXiv preprint arXiv:2310.01655*, 2023.
- [16] Jiayu Ding, Shuming Ma, Li Dong, Xingxing Zhang, Shaohan Huang, Wenhui Wang, Nanning Zheng, and Furu Wei. Longnet: Scaling transformers to 1,000,000,000 tokens. *arXiv preprint arXiv:2307.02486*, 2023.
- [17] Beidi Chen, Tri Dao, Eric Winsor, Zhao Song, Atri Rudra, and Christopher Ré. Scatterbrain: Unifying sparse and low-rank attention. In A. Beygelzimer, Y. Dauphin, P. Liang, and J. Wortman Vaughan, editors, *Advances in Neural Information Processing Systems*, 2021. URL <https://openreview.net/forum?id=SehIKudiIo1>.
- [18] Tri Dao, Beidi Chen, Nimit S Sohoni, Arjun Desai, Michael Poli, Jessica Grogan, Alexander Liu, Aniruddh Rao, Atri Rudra, and Christopher Ré. Monarch: Expressive structured matrices for efficient and accurate training. In *International Conference on Machine Learning*, pages 4690–4721. PMLR, 2022.
- [19] Albert Gu, Karan Goel, and Christopher Re. Efficiently modeling long sequences with structured state spaces. In *International Conference on Learning Representations*, 2022. URL <https://openreview.net/forum?id=uYLFoz1v1AC>.
- [20] Jimmy T.H. Smith, Andrew Warrington, and Scott Linderman. Simplified state space layers for sequence modeling. In *The Eleventh International Conference on Learning Representations*, 2023. URL <https://openreview.net/forum?id=Ai8Hw3AXqks>.
- [21] Daniel Y Fu, Tri Dao, Khaled Kamal Saab, Armin W Thomas, Atri Rudra, and Christopher Re. Hungry hungry hippos: Towards language modeling with state space models. In *The Eleventh International Conference on Learning Representations*, 2023. URL <https://openreview.net/forum?id=COZDy0WYGg>.
- [22] Jimmy T.H. Smith, Shalini De Mello, Jan Kautz, Scott Linderman, and Wonmin Byeon. Convolutional state space models for long-range spatiotemporal modeling. In *Thirty-seventh Conference on Neural Information Processing Systems*, 2023. URL <https://openreview.net/forum?id=1ZvEtnrHS1>.
- [23] Albert Gu, Tri Dao, Stefano Ermon, Atri Rudra, and Christopher Ré. Hippo: Recurrent memory with optimal polynomial projections. *Advances in neural information processing systems*, 33:1474–1487, 2020.
- [24] Badri N. Patro and Vijay S. Agneeswaran. Simba: Simplified mamba-based architecture for vision and multivariate time series, 2024.
- [25] Badri Narayana Patro and Vijay Srinivas Agneeswaran. Mamba-360: Survey of state space models as transformer alternative for long sequence modelling: Methods, applications, and challenges. *arXiv preprint arXiv:2404.16112*, 2024.
- [26] Masanao Aoki. *State space modeling of time series*. Springer Science & Business Media, 2013.
- [27] Michael Zhang, Khaled Kamal Saab, Michael Poli, Tri Dao, Karan Goel, and Christopher Re. Effectively modeling time series with simple discrete state spaces. In *The Eleventh International Conference on Learning Representations*, 2023. URL <https://openreview.net/forum?id=2EpjkjzdCAa>.
- [28] Eric Martin and Chris Cundy. Parallelizing linear recurrent neural nets over sequence length. In *International Conference on Learning Representations*, 2018. URL <https://openreview.net/forum?id=HyUNwulC->.

- [29] Albert Gu, Karan Goel, Ankit Gupta, and Christopher Ré. On the parameterization and initialization of diagonal state space models. In Alice H. Oh, Alekh Agarwal, Danielle Belgrave, and Kyunghyun Cho, editors, *Advances in Neural Information Processing Systems*, 2022. URL <https://openreview.net/forum?id=yJE7iQSAep>.
- [30] Zhuang Liu, Hanzi Mao, Chao-Yuan Wu, Christoph Feichtenhofer, Trevor Darrell, and Saining Xie. A convnet for the 2020s. In *Proceedings of the IEEE/CVF conference on computer vision and pattern recognition*, pages 11976–11986, 2022.
- [31] Zequn Qin, Pengyi Zhang, Fei Wu, and Xi Li. Fcanet: Frequency channel attention networks. In *Proceedings of the IEEE/CVF international conference on computer vision*, pages 783–792, 2021.
- [32] Si-An Chen, Chun-Liang Li, Nate Yoder, Sercan O Arik, and Tomas Pfister. Tsmixer: An all-mlp architecture for time series forecasting. *arXiv preprint arXiv:2303.06053*, 2023.
- [33] Noam Shazeer. Glu variants improve transformer. *arXiv preprint arXiv:2002.05202*, 2020.
- [34] Zhen Qin, Songlin Yang, and Yiran Zhong. Hierarchically gated recurrent neural network for sequence modeling. In *Thirty-seventh Conference on Neural Information Processing Systems*, 2023. URL <https://openreview.net/forum?id=P1TCHxJwLB>.
- [35] Ameen Ali, Itamar Zimmerman, and Lior Wolf. The hidden attention of mamba models. *arXiv preprint arXiv:2403.01590*, 2024.
- [36] Albert Gu. *Modeling Sequences with Structured State Spaces*. Stanford University, 2023.
- [37] Junxiong Wang, Jing Nathan Yan, Albert Gu, and Alexander Rush. Pretraining without attention. In Houda Bouamor, Juan Pino, and Kalika Bali, editors, *Findings of the Association for Computational Linguistics: EMNLP 2023*, pages 58–69, Singapore, December 2023. Association for Computational Linguistics. doi: 10.18653/v1/2023.findings-emnlp.5. URL <https://aclanthology.org/2023.findings-emnlp.5>.
- [38] Ali Behrouz and Farnoosh Hashemi. Graph mamba: Towards learning on graphs with state space models. *arXiv preprint arXiv:2402.08678*, 2024.
- [39] Clément Pernet, Hippolyte Signargout, and Gilles Villard. Exact computations with quasiseparable matrices. In *Proceedings of the 2023 International Symposium on Symbolic and Algebraic Computation*, pages 480–489, 2023.
- [40] Clément Pernet. Computing with quasiseparable matrices. In *Proceedings of the ACM on International Symposium on Symbolic and Algebraic Computation*, ISSAC ’16. ACM, July 2016. doi: 10.1145/2930889.2930915. URL <http://dx.doi.org/10.1145/2930889.2930915>.
- [41] Yue Liu, Yunjie Tian, Yuzhong Zhao, Hongtian Yu, Lingxi Xie, Yaowei Wang, Qixiang Ye, and Yunfan Liu. Vmamba: Visual state space model. *arXiv preprint arXiv:2401.10166*, 2024.
- [42] Mingyu Ding, Bin Xiao, Noel Codella, Ping Luo, Jingdong Wang, and Lu Yuan. Davit: Dual attention vision transformers. In *European conference on computer vision*, pages 74–92. Springer, 2022.
- [43] Jun Fu, Jing Liu, Haijie Tian, Yong Li, Yongjun Bao, Zhiwei Fang, and Hanqing Lu. Dual attention network for scene segmentation. In *Proceedings of the IEEE/CVF conference on computer vision and pattern recognition*, pages 3146–3154, 2019.
- [44] Songlin Yang, Bailin Wang, Yikang Shen, Rameswar Panda, and Yoon Kim. Gated linear attention transformers with hardware-efficient training. In *International conference on machine learning (ICML)*, 2024.
- [45] Mohammed Muqeeth, Haokun Liu, and Colin Raffel. Soft merging of experts with adaptive routing. *Transactions on Machine Learning Research*, 2024. URL <https://openreview.net/forum?id=7I1991c54z>.

- [46] Carlos Riquelme, Joan Puigcerver, Basil Mustafa, Maxim Neumann, Rodolphe Jenatton, André Susano Pinto, Daniel Keysers, and Neil Houlsby. Scaling vision with sparse mixture of experts. *Advances in Neural Information Processing Systems*, 34:8583–8595, 2021.
- [47] Eric Nguyen, Karan Goel, Albert Gu, Gordon Downs, Preey Shah, Tri Dao, Stephen Baccus, and Christopher Ré. S4nd: Modeling images and videos as multidimensional signals with state spaces. *Advances in neural information processing systems*, 35:2846–2861, 2022.
- [48] Chunlong Xia, Xinliang Wang, Feng Lv, Xin Hao, and Yifeng Shi. Vit-comer: Vision transformer with convolutional multi-scale feature interaction for dense predictions. *Computer Vision and Pattern Recognition (CVPR)*, 2024.
- [49] Jia Deng, Wei Dong, Richard Socher, Li-Jia Li, Kai Li, and Li Fei-Fei. Imagenet: A large-scale hierarchical image database. In *2009 IEEE conference on computer vision and pattern recognition*, pages 248–255. Ieee, 2009.
- [50] Kaiming He, Xiangyu Zhang, Shaoqing Ren, and Jian Sun. Deep residual learning for image recognition. In *Proceedings of the IEEE Conference on Computer Vision and Pattern Recognition (CVPR)*, June 2016.
- [51] Ilija Radosavovic, Raj Prateek Kosaraju, Ross Girshick, Kaiming He, and Piotr Dollár. Designing network design spaces. In *Proceedings of the IEEE/CVF conference on computer vision and pattern recognition*, pages 10428–10436, 2020.
- [52] Mingxing Tan and Quoc V. Le. Efficientnet: Rethinking model scaling for convolutional neural networks. In *ICML*, pages 6105–6114, 2019.
- [53] Ao Wang, Hui Chen, Zijia Lin, Jungong Han, and Guiguang Ding. Repvit: Revisiting mobile cnn from vit perspective. In *Proceedings of the IEEE Conference on Computer Vision and Pattern Recognition (CVPR)*, 2024.
- [54] Hugo Touvron, Matthieu Cord, Matthijs Douze, Francisco Massa, Alexandre Sablayrolles, and Hervé Jégou. Training data-efficient image transformers & distillation through attention. In *International conference on machine learning*, pages 10347–10357. PMLR, 2021.
- [55] Ze Liu, Yutong Lin, Yue Cao, Han Hu, Yixuan Wei, Zheng Zhang, Stephen Lin, and Baining Guo. Swin transformer: Hierarchical vision transformer using shifted windows. In *Proceedings of the IEEE/CVF international conference on computer vision*, pages 10012–10022, 2021.
- [56] Ze Liu, Han Hu, Yutong Lin, Zhuliang Yao, Zhenda Xie, Yixuan Wei, Jia Ning, Yue Cao, Zheng Zhang, Li Dong, et al. Swin transformer v2: Scaling up capacity and resolution. In *Proceedings of the IEEE/CVF conference on computer vision and pattern recognition*, pages 12009–12019, 2022.
- [57] Chenyang Si, Weihao Yu, Pan Zhou, Yichen Zhou, Xinchao Wang, and Shuicheng Yan. Inception transformer. *Advances in Neural Information Processing Systems*, 35:23495–23509, 2022.
- [58] Sachin Mehta and Mohammad Rastegari. Mobilevit: Light-weight, general-purpose, and mobile-friendly vision transformer. In *International Conference on Learning Representations*, 2022. URL <https://openreview.net/forum?id=vh-0sUt8HlG>.
- [59] Yanyu Li, Geng Yuan, Yang Wen, Ju Hu, Georgios Evangelidis, Sergey Tulyakov, Yanzhi Wang, and Jian Ren. Efficientformer: Vision transformers at mobilenet speed. *Advances in Neural Information Processing Systems*, 35:12934–12949, 2022.
- [60] Xu Ma, Xiyang Dai, Jianwei Yang, Bin Xiao, Yinpeng Chen, Yun Fu, and Lu Yuan. Efficient modulation for vision networks. In *The Twelfth International Conference on Learning Representations*, 2024. URL <https://openreview.net/forum?id=ip5LHJs6QX>.
- [61] Pavan Kumar Anasosalu Vasu, James Gabriel, Jeff Zhu, Oncel Tuzel, and Anurag Ranjan. Fastvit: A fast hybrid vision transformer using structural reparameterization. In *Proceedings of the IEEE/CVF International Conference on Computer Vision*, pages 5785–5795, 2023.

- [62] Qihang Fan, Huaibo Huang, Xiaoqiang Zhou, and Ran He. Lightweight vision transformer with bidirectional interaction. *Advances in Neural Information Processing Systems*, 36, 2023.
- [63] Michael Poli, Stefano Massaroli, Eric Nguyen, Daniel Y Fu, Tri Dao, Stephen Baccus, Yoshua Bengio, Stefano Ermon, and Christopher Ré. Hyena hierarchy: Towards larger convolutional language models. In *International Conference on Machine Learning*, pages 28043–28078. PMLR, 2023.
- [64] Tao Huang, Xiaohuan Pei, Shan You, Fei Wang, Chen Qian, and Chang Xu. Localmamba: Visual state space model with windowed selective scan. *arXiv preprint arXiv:2403.09338*, 2024.
- [65] Ting Yao, Yingwei Pan, Yehao Li, Chong-Wah Ngo, and Tao Mei. Wave-vit: Unifying wavelet and transformers for visual representation learning. In *European Conference on Computer Vision*, pages 328–345. Springer, 2022.
- [66] Mostafa Dehghani, Basil Mustafa, Josip Djolonga, Jonathan Heek, Matthias Minderer, Mathilde Caron, Andreas Peter Steiner, Joan Puigcerver, Robert Geirhos, Ibrahim Alabdulmohsin, Avital Oliver, Piotr Padlewski, Alexey A. Gritsenko, Mario Lucic, and Neil Houlsby. Patch n’ pack: Navit, a vision transformer for any aspect ratio and resolution. In *Thirty-seventh Conference on Neural Information Processing Systems*, 2023. URL <https://openreview.net/forum?id=VpGFHmI7e5>.
- [67] Tete Xiao, Yingcheng Liu, Bolei Zhou, Yuning Jiang, and Jian Sun. Unified perceptual parsing for scene understanding. In *ECCV*, pages 418–434, 2018.
- [68] Wenhai Wang, Enze Xie, Xiang Li, Deng-Ping Fan, Kaitao Song, Ding Liang, Tong Lu, Ping Luo, and Ling Shao. Pvt v2: Improved baselines with pyramid vision transformer. *Computational Visual Media*, 8(3):415–424, 2022.
- [69] Tsung-Yi Lin, Michael Maire, Serge Belongie, James Hays, Pietro Perona, Deva Ramanan, Piotr Dollár, and C Lawrence Zitnick. Microsoft coco: Common objects in context. In *Computer Vision—ECCV 2014: 13th European Conference, Zurich, Switzerland, September 6–12, 2014, Proceedings, Part V 13*, pages 740–755. Springer, 2014.
- [70] Prajit Ramachandran, Barret Zoph, and Quoc V Le. Searching for activation functions. *arXiv preprint arXiv:1710.05941*, 2017.
- [71] Hugo Touvron, Thibaut Lavril, Gautier Izacard, Xavier Martinet, Marie-Anne Lachaux, Timothée Lacroix, Baptiste Rozière, Naman Goyal, Eric Hambro, Faisal Azhar, et al. Llama: Open and efficient foundation language models. *arXiv preprint arXiv:2302.13971*, 2023.
- [72] Jun Ma, Feifei Li, and Bo Wang. U-mamba: Enhancing long-range dependency for biomedical image segmentation. *arXiv preprint arXiv:2401.04722*, 2024.
- [73] Vincent Tao Hu, Stefan Andreas Baumann, Ming Gui, Olga Grebenkova, Pingchuan Ma, Johannes Fischer, and Bjorn Ommer. Zigma: Zigzag mamba diffusion model. *arXiv preprint arXiv:2403.13802*, 2024.
- [74] Yair Schiff, Chia-Hsiang Kao, Aaron Gokaslan, Tri Dao, Albert Gu, and Volodymyr Kuleshov. Caduceus: Bi-directional equivariant long-range dna sequence modeling. *arXiv preprint arXiv:2403.03234*, 2024.
- [75] Guo Chen, Yifei Huang, Jilan Xu, Baoqi Pei, Zhe Chen, Zhiqi Li, Jiahao Wang, Kunchang Li, Tong Lu, and Limin Wang. Video mamba suite: State space model as a versatile alternative for video understanding. *arXiv preprint arXiv:2403.09626*, 2024.
- [76] Shufan Li, Harkanwar Singh, and Aditya Grover. Mamba-nd: Selective state space modeling for multi-dimensional data. *arXiv preprint arXiv:2402.05892*, 2024.
- [77] Ali Behrouz and Farnoosh Hashemi. Brain-mamba: Encoding brain activity via selective state space models. In *Conference on Health, Inference, and Learning*. PMLR, 2024.

- [78] Dan Hendrycks and Kevin Gimpel. Gaussian error linear units (gelus). *arXiv preprint arXiv:1606.08415*, 2016.
- [79] Angelos Katharopoulos, Apoorv Vyas, Nikolaos Pappas, and François Fleuret. Transformers are rnns: Fast autoregressive transformers with linear attention. In *International conference on machine learning*, pages 5156–5165. PMLR, 2020.
- [80] Mahdi Karami and Ali Ghodsi. Orchid: Flexible and data-dependent convolution for sequence modeling. *arXiv preprint arXiv:2402.18508*, 2024.
- [81] Soham De, Samuel L Smith, Anushan Fernando, Aleksandar Botev, George Cristian-Muraru, Albert Gu, Ruba Haroun, Leonard Berrada, Yutian Chen, Srivatsan Srinivasan, et al. Griffin: Mixing gated linear recurrences with local attention for efficient language models. *arXiv preprint arXiv:2402.19427*, 2024.
- [82] Alex Krizhevsky, Ilya Sutskever, and Geoffrey E Hinton. Imagenet classification with deep convolutional neural networks. *Advances in neural information processing systems*, 25, 2012.
- [83] Axel Pinz et al. Object categorization. *Foundations and Trends® in Computer Graphics and Vision*, 1(4):255–353, 2006.
- [84] Sergey Ioffe and Christian Szegedy. Batch normalization: Accelerating deep network training by reducing internal covariate shift. In *International conference on machine learning*, pages 448–456. pmlr, 2015.
- [85] Saining Xie, Ross Girshick, Piotr Dollár, Zhuowen Tu, and Kaiming He. Aggregated residual transformations for deep neural networks. In *Proceedings of the IEEE conference on computer vision and pattern recognition*, pages 1492–1500, 2017.
- [86] Baoyuan Liu, Min Wang, Hassan Foroosh, Marshall Tappen, and Marianna Pensky. Sparse convolutional neural networks. In *Proceedings of the IEEE conference on computer vision and pattern recognition*, pages 806–814, 2015.
- [87] Yunhui Guo, Yandong Li, Liqiang Wang, and Tajana Rosing. Depthwise convolution is all you need for learning multiple visual domains. In *Proceedings of the AAAI Conference on Artificial Intelligence*, volume 33, pages 8368–8375, 2019.
- [88] Ziyu Wang, Wenhao Jiang, Yiming M Zhu, Li Yuan, Yibing Song, and Wei Liu. Dynamixer: a vision mlp architecture with dynamic mixing. In *International conference on machine learning*, pages 22691–22701. PMLR, 2022.
- [89] Chuanxin Tang, Yucheng Zhao, Guangting Wang, Chong Luo, Wenxuan Xie, and Wenjun Zeng. Sparse mlp for image recognition: Is self-attention really necessary? In *Proceedings of the AAAI conference on artificial intelligence*, volume 36, pages 2344–2351, 2022.
- [90] Zheyuan Liu, Cristian Rodriguez-Opazo, Damien Teney, and Stephen Gould. Image retrieval on real-life images with pre-trained vision-and-language models. In *Proceedings of the IEEE/CVF International Conference on Computer Vision*, pages 2125–2134, 2021.
- [91] Syed Waqas Zamir, Aditya Arora, Salman Khan, Munawar Hayat, Fahad Shahbaz Khan, and Ming-Hsuan Yang. Restormer: Efficient transformer for high-resolution image restoration. In *Proceedings of the IEEE/CVF conference on computer vision and pattern recognition*, pages 5728–5739, 2022.
- [92] Hang Zhang, Chongruo Wu, Zhongyue Zhang, Yi Zhu, Haibin Lin, Zhi Zhang, Yue Sun, Tong He, Jonas Mueller, R Manmatha, et al. Resnest: Split-attention networks. In *Proceedings of the IEEE/CVF conference on computer vision and pattern recognition*, pages 2736–2746, 2022.
- [93] Haixu Wu, Jiehui Xu, Jianmin Wang, and Mingsheng Long. Autoformer: Decomposition transformers with auto-correlation for long-term series forecasting. *Advances in neural information processing systems*, 34:22419–22430, 2021.

- [94] Romain Ilbert, Ambroise Odonnat, Vasilii Feofanov, Aladin Virmaux, Giuseppe Paolo, Themis Palpanas, and Ievgen Redko. Unlocking the potential of transformers in time series forecasting with sharpness-aware minimization and channel-wise attention. *arXiv preprint arXiv:2402.10198*, 2024.
- [95] Yuqi Nie, Nam H Nguyen, Phanwadee Sinthong, and Jayant Kalagnanam. A time series is worth 64 words: Long-term forecasting with transformers. In *The Eleventh International Conference on Learning Representations*, 2023. URL <https://openreview.net/forum?id=Jbdc0vT0col>.
- [96] Tian Zhou, Ziqing Ma, Qingsong Wen, Liang Sun, Tao Yao, Wotao Yin, Rong Jin, et al. Film: Frequency improved legendre memory model for long-term time series forecasting. *Advances in Neural Information Processing Systems*, 35:12677–12690, 2022.
- [97] Tian Zhou, Ziqing Ma, Qingsong Wen, Xue Wang, Liang Sun, and Rong Jin. Fedformer: Frequency enhanced decomposed transformer for long-term series forecasting. In *International conference on machine learning*, pages 27268–27286. PMLR, 2022.
- [98] Ekin D Cubuk, Barret Zoph, Jonathon Shlens, and Quoc V Le. Randaugment: Practical automated data augmentation with a reduced search space. In *Proceedings of the IEEE/CVF conference on computer vision and pattern recognition workshops*, pages 702–703, 2020.
- [99] Hongyi Zhang, Moustapha Cisse, Yann N. Dauphin, and David Lopez-Paz. mixup: Beyond empirical risk minimization. In *International Conference on Learning Representations*, 2018. URL <https://openreview.net/forum?id=r1Ddp1-Rb>.
- [100] Sangdoon Yun, Dongyoon Han, Seong Joon Oh, Sanghyuk Chun, Junsuk Choe, and Youngjoon Yoo. Cutmix: Regularization strategy to train strong classifiers with localizable features. In *Proceedings of the IEEE/CVF international conference on computer vision*, pages 6023–6032, 2019.
- [101] Zhun Zhong, Liang Zheng, Guoliang Kang, Shaozi Li, and Yi Yang. Random erasing data augmentation. In *Proceedings of the AAAI conference on artificial intelligence*, volume 34, pages 13001–13008, 2020.
- [102] Dan Hendrycks, Norman Mu, Ekin Dogus Cubuk, Barret Zoph, Justin Gilmer, and Balaji Lakshminarayanan. Augmix: A simple method to improve robustness and uncertainty under data shift. In *International Conference on Learning Representations*, 2020. URL <https://openreview.net/forum?id=S1gmrxFvB>.
- [103] Jiaxin Shi, Ke Alexander Wang, and Emily Fox. Sequence modeling with multiresolution convolutional memory. In *International Conference on Machine Learning*, pages 31312–31327. PMLR, 2023.
- [104] Kai Chen, Jiaqi Wang, Jiangmiao Pang, Yuhang Cao, Yu Xiong, Xiaoxiao Li, Shuyang Sun, Wansen Feng, Ziwei Liu, Jiarui Xu, et al. Mmdetection: Open mmlab detection toolbox and benchmark. *arXiv preprint arXiv:1906.07155*, 2019.
- [105] Bolei Zhou, Hang Zhao, Xavier Puig, Tete Xiao, Sanja Fidler, Adela Barriuso, and Antonio Torralba. Semantic understanding of scenes through the ade20k dataset. *International Journal of Computer Vision*, 127:302–321, 2019.
- [106] Tete Xiao, Yingcheng Liu, Bolei Zhou, Yuning Jiang, and Jian Sun. Unified perceptual parsing for scene understanding. In *Proceedings of the European conference on computer vision (ECCV)*, pages 418–434, 2018.
- [107] Ilya Loshchilov and Frank Hutter. Decoupled weight decay regularization. In *International Conference on Learning Representations*, 2019. URL <https://openreview.net/forum?id=Bkg6RiCqY7>.
- [108] Alireza Fathi, Xiaofeng Ren, and James M Rehg. Learning to recognize objects in egocentric activities. In *CVPR 2011*, pages 3281–3288. IEEE, 2011.



- [109] Hang Zhao, Antonio Torralba, Lorenzo Torresani, and Zhicheng Yan. Hacs: Human action clips and segments dataset for recognition and temporal localization. In *Proceedings of the IEEE/CVF International Conference on Computer Vision*, pages 8668–8678, 2019.
- [110] Chen-Lin Zhang, Jianxin Wu, and Yin Li. Actionformer: Localizing moments of actions with transformers. In *European Conference on Computer Vision*, pages 492–510. Springer, 2022.
- [111] Fangqiu Yi, Hongyu Wen, and Tingting Jiang. Asformer: Transformer for action segmentation. In *The British Machine Vision Conference (BMVC)*, 2021.
- [112] Krzysztof Marcin Choromanski, Valerii Likhoshesterov, David Dohan, Xingyou Song, Andreea Gane, Tamas Sarlos, Peter Hawkins, Jared Quincy Davis, Afroz Mohiuddin, Lukasz Kaiser, David Benjamin Belanger, Lucy J Colwell, and Adrian Weller. Rethinking attention with performers. In *International Conference on Learning Representations*, 2021. URL <https://openreview.net/forum?id=Ua6zuk0WRH>.
- [113] Eric Brill and Robert C Moore. An improved error model for noisy channel spelling correction. In *Proceedings of the 38th annual meeting of the association for computational linguistics*, pages 286–293, 2000.
- [114] Yazan Abu Farha and Jurgen Gall. Ms-tcn: Multi-stage temporal convolutional network for action segmentation. In *Proceedings of the IEEE/CVF conference on computer vision and pattern recognition*, pages 3575–3584, 2019.
- [115] Shiyang Li, Xiaoyong Jin, Yao Xuan, Xiyu Zhou, Wenhui Chen, Yu-Xiang Wang, and Xifeng Yan. Enhancing the locality and breaking the memory bottleneck of transformer on time series forecasting. *Advances in neural information processing systems*, 32, 2019.
- [116] John R Hershey, Zhuo Chen, Jonathan Le Roux, and Shinji Watanabe. Deep clustering: Discriminative embeddings for segmentation and separation. In *2016 IEEE international conference on acoustics, speech and signal processing (ICASSP)*, pages 31–35. IEEE, 2016.
- [117] Xilin Jiang, Cong Han, and Nima Mesgarani. Dual-path mamba: Short and long-term bidirectional selective structured state space models for speech separation. *arXiv preprint arXiv:2403.18257*, 2024.
- [118] Yi Luo and Nima Mesgarani. Conv-tasnet: Surpassing ideal time–frequency magnitude masking for speech separation. *IEEE/ACM transactions on audio, speech, and language processing*, 27(8):1256–1266, 2019.
- [119] Efthymios Tzinis, Zhepei Wang, Xilin Jiang, and Paris Smaragdis. Compute and memory efficient universal sound source separation. *Journal of Signal Processing Systems*, 94(2): 245–259, 2022.
- [120] Neil Zeghidour and David Grangier. Wavesplit: End-to-end speech separation by speaker clustering. *IEEE/ACM Transactions on Audio, Speech, and Language Processing*, 29:2840–2849, 2021.
- [121] Yi Luo and Nima Mesgarani. Tasnet: time-domain audio separation network for real-time, single-channel speech separation. In *2018 IEEE International Conference on Acoustics, Speech and Signal Processing (ICASSP)*, pages 696–700. IEEE, 2018.
- [122] Yi Luo, Zhuo Chen, and Takuya Yoshioka. Dual-path rnn: efficient long sequence modeling for time-domain single-channel speech separation. In *ICASSP 2020-2020 IEEE International Conference on Acoustics, Speech and Signal Processing (ICASSP)*, pages 46–50. IEEE, 2020.
- [123] Eliya Nachmani, Yossi Adi, and Lior Wolf. Voice separation with an unknown number of multiple speakers. In *International Conference on Machine Learning*, pages 7164–7175. PMLR, 2020.
- [124] Jingjing Chen, Qirong Mao, and Dong Liu. Dual-Path Transformer Network: Direct Context-Aware Modeling for End-to-End Monaural Speech Separation. In *Proc. Interspeech 2020*, pages 2642–2646, 2020. doi: 10.21437/Interspeech.2020-2205.

- [125] Cem Subakan, Mirco Ravanelli, Samuele Cornell, Mirko Bronzi, and Jianyuan Zhong. Attention is all you need in speech separation. In *ICASSP 2021-2021 IEEE International Conference on Acoustics, Speech and Signal Processing (ICASSP)*, pages 21–25. IEEE, 2021.
- [126] Joel Rixen and Matthias Renz. QDPN - Quasi-dual-path Network for single-channel Speech Separation. In *Proc. Interspeech 2022*, pages 5353–5357, 2022. doi: 10.21437/Interspeech.2022-700.
- [127] Shengkui Zhao and Bin Ma. Mossformer: Pushing the performance limit of monaural speech separation using gated single-head transformer with convolution-augmented joint self-attentions. In *ICASSP 2023-2023 IEEE International Conference on Acoustics, Speech and Signal Processing (ICASSP)*, pages 1–5. IEEE, 2023.
- [128] William Ravenscroft, Stefan Goetze, and Thomas Hain. On time domain conformer models for monaural speech separation in noisy reverberant acoustic environments. In *2023 IEEE Automatic Speech Recognition and Understanding Workshop (ASRU)*, pages 1–7. IEEE, 2023.
- [129] Shahar Lutati, Eliya Nachmani, and Lior Wolf. Separate and diffuse: Using a pretrained diffusion model for better source separation. In *The Twelfth International Conference on Learning Representations*, 2024. URL <https://openreview.net/forum?id=UXALv01JZS>.
- [130] Shengkui Zhao, Yukun Ma, Chongjia Ni, Chong Zhang, Hao Wang, Trung Hieu Nguyen, Kun Zhou, Jiaqi Yip, Dianwen Ng, and Bin Ma. Mossformer2: Combining transformer and rnn-free recurrent network for enhanced time-domain monaural speech separation, 2023.
- [131] Chen Chen, Chao-Han Huck Yang, Kai Li, Yuchen Hu, Pin-Jui Ku, and Eng Siong Chng. A neural state-space model approach to efficient speech separation, 2023.
- [132] Xiaosong Zhang, Yunjie Tian, Lingxi Xie, Wei Huang, Qi Dai, Qixiang Ye, and Qi Tian. Hivit: A simpler and more efficient design of hierarchical vision transformer. In *The Eleventh International Conference on Learning Representations*, 2023.
- [133] Wenxiao Wang, Lu Yao, Long Chen, Binbin Lin, Deng Cai, Xiaofei He, and Wei Liu. Cross-former: A versatile vision transformer hinging on cross-scale attention. In *ICLR*, 2022.
- [134] Shitao Tang, Jiahui Zhang, Siyu Zhu, et al. Quadtree attention for vision transformers. In *ICLR*, 2022.
- [135] Yongming Rao, Wenliang Zhao, Yansong Tang, Jie Zhou, Ser-Lam Lim, and Jiwen Lu. Hornet: Efficient high-order spatial interactions with recursive gated convolutions. *NeurIPS*, 2022.
- [136] Alaaeldin El-Nouby, Hugo Touvron, Mathilde Caron, et al. Xcit: Cross-covariance image transformers. In *NeurIPS*, 2021.
- [137] Kunchang Li, Yali Wang, Peng Gao, et al. Uniformer: Unified transformer for efficient spatial-temporal representation learning. In *ICLR*, 2022.
- [138] Youngwan Lee, Jonghee Kim, Jeffrey Willette, and Sung Ju Hwang. Mpvit: Multi-path vision transformer for dense prediction. In *CVPR*, 2022.

## A Backgrounds

### A.1 State Space Models

SSMs are known as linear time-invariant systems that map input sequence  $x(t) \in \mathbb{R}^L$  to response sequence  $y(t) \in \mathbb{R}^L$  [26]. To this end, SSMs use a latent state  $h(t) \in \mathbb{R}^{N \times L}$ , parameter  $\mathbf{A} \in \mathbb{R}^{N \times N}$ , and projection parameters  $\mathbf{B} \in \mathbb{R}^{N \times 1}$ ,  $\mathbf{C} \in \mathbb{R}^{1 \times N}$  such that:

$$h'(t) = \mathbf{A} h(t) + \mathbf{B} x(t), \quad y(t) = \mathbf{C} h(t). \quad (12)$$

To adapt these models to deep learning settings, the first step is to discretize the signals  $\mathbf{A}$ ,  $\mathbf{B}$ , and  $\mathbf{C}$ . discrete space state models [23, 27] suggests discretizing the above system using a parameter  $\Delta$  and zero-order hold, i.e.,

$$h_t = \bar{\mathbf{A}} h_{t-1} + \bar{\mathbf{B}} x_t, \quad y_t = \mathbf{C} h_t, \quad (13)$$

where  $\bar{\mathbf{A}} = \exp(\Delta \mathbf{A})$  and  $\bar{\mathbf{B}} = (\Delta \mathbf{A})^{-1} (\exp(\Delta \mathbf{A}) - I) \cdot \Delta \mathbf{B}$ .

Discrete SSMs can be interpreted as both convolutions and recurrent networks and are equivalent to the following convolution [23]:

$$\begin{aligned} \bar{\mathbf{K}} &= (\mathbf{C}\bar{\mathbf{B}}, \mathbf{C}\bar{\mathbf{A}}\bar{\mathbf{B}}, \dots, \mathbf{C}\bar{\mathbf{A}}^{L-1}\bar{\mathbf{B}}), \\ y &= x * \bar{\mathbf{K}}, \end{aligned} \quad (14)$$

which makes them very efficient in both training, as a convolution, and inference, as an recurrent model. Discrete SSMs, however, are based on data-independent parameters, meaning that parameters  $\bar{\mathbf{A}}$ ,  $\bar{\mathbf{B}}$ , and  $\mathbf{C}$  are time invariant and are the same for any input, limiting their effectiveness in compressing context into a smaller state [8]. To alleviate this limitation, recently, Gu and Dao [8] present a selective SSMs (S6) block that effectively selects relevant context by enabling dependence of the parameters  $\bar{\mathbf{B}}$ ,  $\bar{\mathbf{C}}$ , and  $\Delta$  on the input  $x_t$ , i.e.:

$$\bar{\mathbf{B}}_t = \text{Linear}_{\mathbf{B}}(x_t) \quad (15)$$

$$\bar{\mathbf{C}}_t = \text{Linear}_{\mathbf{C}}(x_t) \quad (16)$$

$$\Delta_t = \text{Softplus}(\text{Linear}_{\Delta}(x_t)), \quad (17)$$

where  $\text{Linear}(\cdot)$  is a linear projection and  $\text{Softplus}(\cdot) = \log(1 + \exp(\cdot))$ . This data dependency comes at the cost of the model not being able to be trained as a convolution, causing challenges for the model efficiency and scalability. To overcome this challenge, Gu and Dao [8] show that the linear recurrence in Equation 2 can be formulated as an associative scan [28], which accepts efficient parallel algorithms.

### A.2 Mamba

Using the S6 block, Gu and Dao [8] present Mamba architecture that uses a 1D convolution followed by S6 block. Mamba further uses the SiLU/Swish activation function [70] and gated the main branch with a linear layer, resulting in a gating with SwiGLU [71]. That is:

$$\bar{x} = \sigma(\text{Conv}(\text{Linear}(x))), \quad (18)$$

$$\bar{x}_{\text{Gate}} = \text{SiLU}(\text{Linear}(x)), \quad (19)$$

$$\Delta_x = \text{Softplus}(\text{Linear}_{\Delta}(x)), \quad (20)$$

$$\bar{\mathbf{C}}_x = \text{Linear}_{\mathbf{C}}(x), \quad (21)$$

$$\bar{\mathbf{B}}_x = \text{Linear}_{\mathbf{B}}(x), \quad (22)$$

$$y_{\text{Token}} = \text{SSM}_{\bar{\mathbf{A}}, \bar{\mathbf{B}}_x, \mathbf{C}_x, \Delta_x}(\bar{x}) \otimes \bar{x}_{\text{Gate}}. \quad (\text{Using Equation 13}) \quad (23)$$

Mamba has shown promising results in various domains e.g., vision tasks [9, 24, 41, 64, 72], graphs [38], image generation [73], DNA modeling [8, 74], video understanding [25, 75, 76], and brain activity analysis [77].

### A.3 Quasi-Separable Matrices

Quasi-seperable matrices are a class of matrices with structured representations.

**Definition 1** (Quasi-Seperable Matrix [39]). *An  $N \times N$  matrix  $A$  is  $s$ -quasi-seperable if for all  $k \in [1, N]$ , we have:*

$$\text{rank}(A_{1\dots k, k+1\dots n}) \leq s \quad (24)$$

$$\text{rank}(A_{k+1\dots n, 1\dots k}) \leq s. \quad (25)$$

There are different forms for quasi-seperable matrices to be represented [39]. In this paper, we need SSS format.

**Definition 2** ( $t$ -SSS [39]). *Let  $A = \begin{pmatrix} a_{1,1} & \dots & a_{1,p} \\ \vdots & \ddots & \vdots \\ a_{p,1} & \dots & a_{p,p} \end{pmatrix} \in K^{N \times N}$ , with  $t \times t$  blocks  $A_{i,j}$  such that  $p = \frac{N}{t}$ ,*

*$A$  is SSS of order  $t$  ( $t$ -SSS) if it is given by the  $t \times t$  matrices  $(C_i, V_i)$ ,  $(B_i, U_i)$ ,  $(A_i, W_i)$ ,  $D_i$  such that:*

$$A_{i,j} = \begin{cases} C_i R_{i-1} \dots R_{j+1} Q_j & \text{if } i > j \\ D_i & \text{if } i = j \\ U_i W_{i+1} \dots W_{j-1} V_j & \text{if } j < i \end{cases} \quad (26)$$

**Proposition 1** (Pernet et al. [39]). *Any  $N \times N$   $s$ -quasi-seperable has an  $s$ -SSS representation.*

The above proposition makes sure that every learned QSMixer is equivalent to a S6 block as we can define  $C_i = \mathbf{C}_i$ ,  $B_i = \mathbf{B}_i$ ,  $A_i = \mathbf{A}_i$ ,  $V_i = \mathbf{B}_{L-i+1}$ ,  $U_i = \mathbf{C}_{L-i+1}$ , and  $W_i = \mathbf{A}_{L-i+1}$ .

### A.4 MLP-Mixer

MLPMixer [11] is an all MLP architecture that repeatedly mix information along the sequence and model dimensions using MLP layers. The main architecture of MLP mixer consists of two phase: (1) Token Mixer, where the sequence of tokens are mixed using an MLP block, and (2) Channel Mixer, where channels are mixed using an MLP block. Formally, given  $X \in \mathbb{R}^{N \times d}$  as the input, the MLPMixer is defined as:

$$\mathbf{H}_{\text{token}} = \mathbf{X} + \mathbf{W}_{\text{token}}^{(2)} \sigma(\mathbf{W}_{\text{token}}^{(1)} \text{LayerNorm}(\mathbf{X})), \quad (27)$$

$$\mathbf{H}_{\text{channel}} = \mathbf{H}_{\text{token}} + \mathbf{W}_{\text{channel}}^{(2)} \sigma(\mathbf{W}_{\text{channel}}^{(1)} \text{LayerNorm}(\mathbf{H}_{\text{token}})^\top)^\top, \quad (28)$$

where  $\sigma(\cdot)$  is nonlinear activation function (usually GeLU [78]), and  $\mathbf{W}_{\text{token}}^{(1)}$ ,  $\mathbf{W}_{\text{token}}^{(2)}$ ,  $\mathbf{W}_{\text{channel}}^{(1)}$  and  $\mathbf{W}_{\text{channel}}^{(2)}$  are learnable parameters.

### A.5 (Gated) Linear Attention

The Transformer atchitecture [1] uses a softmax attention mechanism which takes an input sequence  $\mathbf{X} \in \mathbb{R}^{N \times d}$ , and computes the output  $\mathbf{O}$  as follows:

$$\mathbf{Q} = \mathbf{X} \mathbf{W}_{\mathbf{Q}} \quad (29)$$

$$\mathbf{K} = \mathbf{X} \mathbf{W}_{\mathbf{K}} \quad (30)$$

$$\mathbf{V} = \mathbf{X} \mathbf{W}_{\mathbf{V}} \quad (31)$$

$$\mathbf{O} = \text{Softmax}\left(\frac{\mathbf{Q}\mathbf{K}^\top}{\sqrt{d}}\right) \mathbf{V}, \quad (32)$$

where  $\mathbf{W}_{\mathbf{Q}}$ ,  $\mathbf{W}_{\mathbf{K}}$ , and  $\mathbf{W}_{\mathbf{V}}$  are learnable parameters. The above equation, during inference, can be re-formulate as:

$$\mathbf{O}_t = \frac{\sum_{i=1}^t \exp(\mathbf{q}_t \mathbf{k}_i^\top) \mathbf{v}_i}{\sum_{i=1}^t \exp(\mathbf{q}_t \mathbf{k}_i^\top)}, \quad (33)$$

where  $\mathbf{q}_i$ ,  $\mathbf{k}_i$ ,  $\mathbf{v}_i$  are the  $i$ -th row of  $\mathbf{Q}$ ,  $\mathbf{K}$ , and  $\mathbf{V}$ , respectively. The above formulation, due to the softmax function, for each  $t$ , requires calculating  $\exp(\mathbf{q}_t \mathbf{k}_i^\top) \mathbf{v}_i$ , resulting in KV cache. To address

this issue, linear attention [79] replaces the softmax with a kernel  $K(x, y) = \langle \phi(x), \phi(y) \rangle$ . Therefore, the calculation of Equation 33 can be simplify to:

$$\mathbf{O}_t = \frac{\sum_{i=1}^t \phi(\mathbf{q}_t) \phi(\mathbf{k}_i)^\top \mathbf{v}_i}{\sum_{i=1}^t \phi(\mathbf{q}_t) \phi(\mathbf{k}_i)^\top} = \frac{\phi(\mathbf{q}_t) \sum_{i=1}^t \phi(\mathbf{k}_i)^\top \mathbf{v}_i}{\phi(\mathbf{q}_t) \sum_{i=1}^t \phi(\mathbf{k}_i)^\top} = \frac{\phi(\mathbf{q}_t) \mathbf{h}_t}{\phi(\mathbf{q}_t) \mathbf{z}_t}, \quad (34)$$

where  $\mathbf{h}_t = \sum_{i=1}^t \phi(\mathbf{k}_i)^\top \mathbf{v}_i$ , and  $\mathbf{z}_t = \sum_{i=1}^t \phi(\mathbf{k}_i)^\top$ , which can be computed as an RNN. In most cases,  $\phi(\cdot)$  is chosen as identity function [44].

The above formulation, however, does not have a decay term or forget gate, making forgetting information difficult for the model. To address this issue, recently, [44] present a gated linear attention with data-dependent forget gate:

$$\mathbf{h}_t = \mathbf{G}_t \odot \mathbf{h}_{t-1} + \mathbf{k}_t^\top \mathbf{v}_t, \quad (35)$$

where  $\mathbf{G}_t \in (0, 1)^{d \times d}$  is the 2D forget gate.

## B Additional Related Work

To situate our contributions in a broader context, we discuss related studies in three groups:

### B.1 Sequence Modeling

Transformers [1] have been the pivotal backbone architecture behind deep learning’s success. Despite their outstanding success in various domains, their attention module has quadratic space and time complexity, which limits their scalability. To this end, recently, several studies aim to design attention-free models with competitive performance to Transformers [80, 81]. To this end, State-space Models (SSMs) have recently emerged as a powerful and attention-free tools for modeling long input sequences [63, 21]. More specifically, recently, Gu and Dao [8] present Mamba, a selective state space model that using input-dependent weights can effectively focus on or ignore some particular tokens. While these sequence models show promising performance on 1D data, they overlook the channel-wise dependencies in sequences. Although this channel-wise dependencies in some tasks on 1D input data like language modeling might not significantly damage the performance, its lackness makes the adaption of these sequence models for multi-dimensional data challenging. Our MambaMixer block uses selective state space models [8] across both channel and tokens to selectively mix and fuse information across these dimensions.

### B.2 Architectures for Generic Vision Backbone

**Convolutional Neural Networks and Mixer Architectures.** CNNs have served as the de-facto standard backbone in computer vision since the AlexNet model [82] outperforms vision models designed based on hand-crafted image features [83]. Several studies have focused on improving the design of CNNs: He et al. [50] present residual networks using skip connection and Ioffe and Szegedy [84] introduce batch normalization, both enabling the design of very deep CNNs. Several studies have focused on using sparse convolutions [85, 86], e.g., depth-wise convolutions [87]. Using the idea of convolutions in the extreme case of small kernels, [11] present MLP-Mixer that use MLP across both patch and channel directions to fuse information in both spatial and feature directions. The success of MLP-Mixer motivated several studies to use matrix multiplication with efficient and sparse matrices across spatial and channel directions [88, 89, 13]. All these architectures, however, are based on data-independent weights, limiting their generalizability and in-context learning ability.

**Vision Transformers.** Motivated by the success of Transformers [1] in various domains, Vision Transformers (ViT) [3] are designed purely based on Transformers. This new backbone architecture has inspired a new paradigm of “isotropic” architectures, which are architectures that use patch embeddings for the first layer and have equal size and shape throughout the network. ViTs due to their ability to learn at scales became popular models over time and various of their variants are designed for a wide array of vision tasks [55, 56, 90, 54]. While many ViT architectures use MLPs for channel mixing, very recently, several studies suggest that a simple MLP is not able to effectively filter irrelevant features and discuss the need of channel-wise attentions [91, 92]. Despite their outstanding performance, Transformers’ time and memory scales quadratic with respect to the

input, making utilizing them challenging for high-resolution images. This is even more challenging, specifically for channel-wise attention in large-networks, where the number of channels is large. Our ViM2 model’s time scales linearly with respect to the input and shows the same pattern for its memory usage. It further uses selective state space models across both channel and token dimension, enabling effectively select (resp. filter) informative (resp. irrelevant) tokens or channels.

**SSM-based Generic Vision Models.** S4ND [47] is pioneer study to employ SSM blocks for visual tasks, handling visual data as continuous signals across 1D, 2D, and 3D domains. Recently, motivated by the success of Mamba [8], Vmamba [41] and Vim [9] adapt Mamba block for generic vision tasks by addressing the directional sensitivity challenge in SSMs based on bi-directional and cross-scan mechanisms. Subsequently, several studies suggest more sophisticated scan mechanisms to improve the performance of these models [76, 64, 73]. Surprisingly, existing adaptations mostly focus on different scanning strategies and treat each channel separately, missing cross-channel dependency. Our ViM2 model, using MambaMixer blocks, can effectively and selectively fuse information across both dimensions.

### B.3 Architectures for Generic Timeseries Backbone

Not surprisingly, Transformer-based models have been common choices for time series forecasting, when modeling the complex relationships of covariates are required [4, 10, 93–95]. Several studies have focused on making the design of Transformers for time series more efficient [4, 93]. Some other studies have focused on extracting long-term information for better forecasting [95, 96]. To this end, Zhou et al. [96] and Zhou et al. [97] suggest decomposing the sequences using Fast Fourier Transformation, enabling better extraction of long-term information. Recently, Chen et al. [32] present TSMixer, an all-MLP architecture for time series forecasting, with state-of-the-art performance and show that to achieve competitive performance in practice, Transformers are not necessarily. Our TSM2, is an alternative MLP- and attention-free architecture that is designed based on MambaMixer block. In this design, S6 blocks, in both directions of variates and time, is used to select (resp. filter) important (resp. irrelevant) variates as well as time stamps.

## C Connection of MambaMixer and Dual-Attentions

We reviewed the concepts of (gated) linear attention in Appendix A. In this section, we discuss the connection of dual-attention methods, e.g., DaViT [42], DANet [43] with MambaMixer and show that if we use linear kernel instead of softmax, then the resulted methods are special cases of MambaMixer. Inspired by Liu et al. [41], we let:

$$\mathbf{V} = [\mathbf{V}_1; \mathbf{V}_2; \dots; \mathbf{V}_L] \in \mathbb{R}^{L \times d_1} : \mathbf{V}_i = \mathbf{x}_i \Delta_i \in \mathbb{R}^{1 \times d_1}, \quad (36)$$

$$\mathbf{K} = [\mathbf{K}_1; \mathbf{K}_2; \dots; \mathbf{K}_L] \in \mathbb{R}^{L \times d_2} : \mathbf{K}_i = \mathbf{B}_i \in \mathbb{R}^{1 \times d_2}, \quad (37)$$

$$\mathbf{Q} = [\mathbf{Q}_1; \mathbf{Q}_2; \dots; \mathbf{Q}_L] \in \mathbb{R}^{L \times d_3} : \mathbf{Q}_i = \mathbf{C}_i \in \mathbb{R}^{1 \times d_3}, \quad (38)$$

$$\mathbf{w} = [\mathbf{w}_1; \dots; \mathbf{w}_L] \in \mathbb{R}^{L \times d_2 \times d_1} : \mathbf{w}_i = \prod_{j=1}^i \exp(A \Delta_j) \in \mathbb{R}^{d_2 \times d_1}, \quad (39)$$

then using the above notation, we can write:

$$\mathbf{y}_i^{(t)} = (\mathbf{Q}_L^{(t)} \odot \mathbf{w}_i^{(t)}) \mathbf{h}_i^{(t)} + \left[ (\mathbf{Q}_L^{(t)} \odot \mathbf{w}_i^{(t)}) \left( \frac{\mathbf{K}^{(t)}}{\mathbf{w}_i^{(t)}} \right)^\top \odot \mathbf{M} \right] \mathbf{V}_i^{(t)}, \quad (40)$$

where  $\mathbf{M} \in \{0, 1\}^{L \times L}$  is the lower triangle mask. Assuming this as a token-wise mixing and then using a channel mixing pass, we have:

$$\mathbf{y}_i^{(c)} = (\mathbf{Q}_L^{(c)} \odot \mathbf{w}_i^{(c)}) \mathbf{h}_i^{(c)} + \left[ (\mathbf{Q}_L^{(c)} \odot \mathbf{w}_i^{(c)}) \left( \frac{\mathbf{K}^{(c)}}{\mathbf{w}_i^{(c)}} \right)^\top \odot \mathbf{M} \right] \mathbf{V}_i^{(c)}. \quad (41)$$

Let  $d_1 = 1$ , i.e., applying the S6 block for each channel separately, both  $\mathbf{y}_i^{(t)}$  and  $\mathbf{y}_i^{(c)}$  are reduced to gated linear attention [44].

## D Fast Matrix-Vector Multiplication of Quasi-Separable Matrices

Inspired by Pernet et al. [39], for fast matrix-vector multiplication, we decompose the quasi-separable matrix  $Q$  into its lower-triangle, upper-triangle, and its diagonal:

$$Q = L + D + U, \quad (42)$$

where  $L_{i,j} = \begin{cases} Q_{i,j} & \text{if } j \leq i \\ 0 & \text{if } i < j \end{cases}$ ,  $L_{i,j} = \begin{cases} 0 & \text{if } j < i \\ Q_{i,j} & \text{if } j = i, \text{ and } \\ 0 & \text{if } i < j \end{cases}$ , and  $U_{i,j} = \begin{cases} Q_{i,j} & \text{if } i < j \\ 0 & \text{if } j \leq i \end{cases}$ . Now, note that

$Qx = Lx + Dx + Ux$ . Fortunately,  $Dx$  can be computed very fast in  $O(N)$  as  $D$  is a diagonal matrix. On the other hand, if we find an efficient algorithm that can perform matrix-vector multiplication for  $L$ , then we can consider  $U^T$  and use the efficient algorithm. So without loss of generality, we focus on

computing  $Lx$ . Note that if we divide matrix  $L$  into smaller windows  $L = \begin{pmatrix} W_{1,1} & W_{1,2} & \dots & W_{1,m} \\ W_{2,1} & W_{2,2} & \dots & W_{2,m} \\ \vdots & \vdots & \ddots & \vdots \\ W_{m,1} & W_{m,2} & \dots & W_{m,m} \end{pmatrix}$ ,

the multiplication can be done in parallel as each window of  $W_{i,j}$  that is completely above the diagonal of the matrix  $L$  is 0 and so the multiplication of vector-matrix is zero. Also, any other window of  $W_{i,j}$  is a low-rank matrix, which has a fast multiplication.

## E Gating with Multi-Resolution Convolutions

As we discussed earlier, we further modified the gating of the MambaMixer and QSMixer to adapt them for vision tasks. That is, we use a set of convolutions to extract multi-resolution features from the input images. We construct features  $F_1, F_2$ , and  $F_3$  with resolution  $\frac{1}{8}, \frac{1}{16}$ , and  $\frac{1}{32}$ , concatenate them, and pass the features to a linear projection layer to construct  $C \in \mathbb{R}^{(\frac{HW}{64} + \frac{HW}{256} + \frac{HW}{1024}) \times D}$ . Next, we use depth-wise separable convolutions with different kernel size  $k_i \times k_i$ , each of which on the features of the same resolution:

$$F_{\text{Conv}} = W_{c_1} \text{DWConv}(W_{c_2} [F_1 || F_2 || F_3]), \quad (43)$$

where  $W_{c_1}$  and  $W_{c_2}$  are learnable parameters. Note that while the original QSMixer and MambaMixer blocks also uses a stack of convolutions, the main change is that instead of applying convolutions on the patched images, we use the stack of convolutions on the multi-resolution image features, without patching. Also, instead of 1D convolutions, here, we use depth-wise separable convolutions.

Now, to gate and combine these features with the main branch (S6 block), we use the modified version of bi-directional fusion module in ViT-CoMer [48] by replacing the attention with linear layers. That is, let  $\mathbf{x}_S$  be the output of the S6 branch and  $F_{\text{Conv}} = [F_{\text{Conv}}^{(1)} || F_{\text{Conv}}^{(2)} || F_{\text{Conv}}^{(3)}]$  are the partitions corresponds to  $F_1, F_2$ , and  $F_3$ , then we have:

$$\mathbf{O} = \text{Linear}([F_{\text{Conv}}^{(1)} || F_{\text{Conv}}^{(2)} + \mathbf{x}_S || F_{\text{Conv}}^{(3)}]), \quad (44)$$

where  $\mathbf{O}$  is the output.

## F Frequently Asked Questions (FAQs)

### F.1 Why Does MambaMixer Work?

MambaMixer and QSMixer are closely connected to dual-linear attentions (see [Theorem 1](#)), and has the ability to filter irrelevant information across both sequence and channels. Their quasi-separable formulation also connect them with mixer methods (e.g., MLP Mixer [11], ConvMixer [12], and M2 [13]), but with the ability of selection, due to the data dependence and discretization process.

### F.2 Why data-dependent Channel Mixing?

Data dependency results in compressing context into a smaller state [8], which is desirable specifically in channel mixing phase. In the discretization process, parameter  $\Delta$  controls the emphasize on the

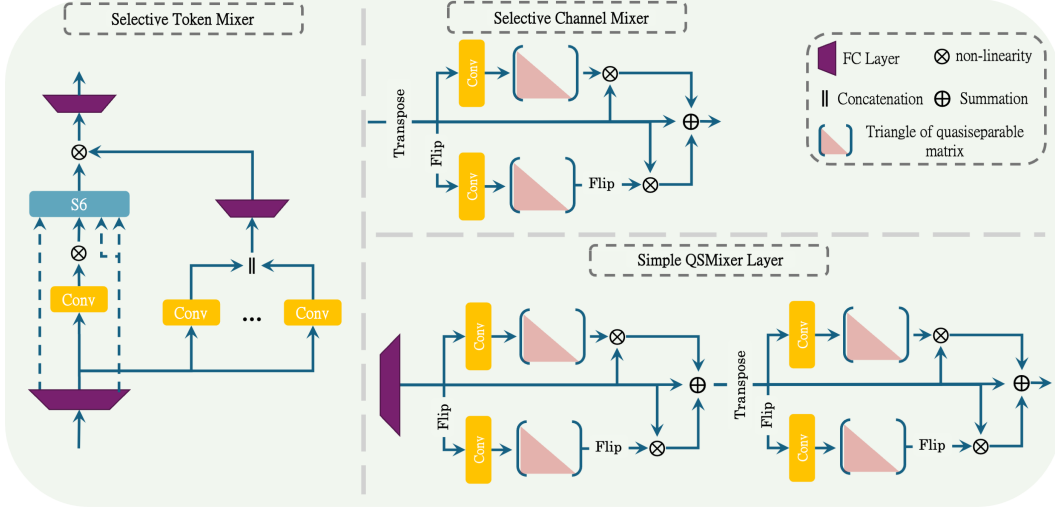


Figure 4: Architectures of Selective Token Mixer, Selective Channel Mixers, and QSMixer.

current input and hidden states. That is, a large value of  $\Delta$  results in only looking at the current input, while a small value of  $\Delta$  results in more emphasize on hidden states. Making parameters, including  $\Delta$ , input-dependent allows each input decides whether the emphasize should be on the hidden states or the current input. Accordingly, it allows to filter irrelevant channels, resulting in a better performance.

### F.3 Visualization of the proposed Architectures

Figure 4 illustrates the architecture of all proposed methods. Layer normalization and residual connections are omitted for the sake of simplicity.

### F.4 Difference of Mamba and Selective Token Mixer in MambaMixer

The main difference of Mamba and the architecture of Selective Token Mixer is its gating with a stack of multi-resolution convolutions. That is, while the gating module of Mamba is fully connected layer, the gating module in selective token mixer is a stack of multi-resolution convolutions, resulting in having multi-resolution view of the data. Another minor difference is that, we make  $\mathbf{B}$ ,  $\mathbf{C}$ , and  $\Delta$  as the functions of the initial input, instead of the function of after convolution. We found this change to be faster than the original design without performance drop.

### F.5 Difference of Mamba and Selective Channel Mixer

Selective channel mixer uses a new form of S6 block based on quasi-separable matrices. Therefore, it does not based on scan and instead uses matrix multiplication algorithms of quasi-separable matrices that can be also parallelizable. To this end, selective channel mixer is non-causal and bi-directional by its nature. Accordingly, it does not require two separate blocks for forward and backward pass. Also, this formulation is more generalized than S6 block as the diagonal elements are not depends on other elements in the matrix, having more representation power (see Figure 1).

### F.6 Difference of Mamba and MambaMixer

In addition to the fact that both selective channel and token mixers have different architectures than Mamba (see Appendices F.4 and F.5), Mamba block treats each channel seperately, while MambaMixer is able to mix channels in a selective manner, meaning that irrelevant channels for each token can be filtered.



## F.7 Difference of VMamba, ViM2, and ViQS

VMamba [41] uses a hierarchical 4 steps architecture by downsampling. It uses Mamba block as a black box model and then using cross-scan module scan the input images in 4 different directions. Moreover, it treat each of the channels separately and does not have channel mixing module. ViM2 and ViQS, on the other hand, use a new architecture of MambaMixer and QSMixer as the backbone. Compared to VMamba, these methods have more ability to capture inter-channel dependencies. Also, while VMamba uses a fix set of scans, ViM2 and ViQS use SoS, which can adaptively learn to use different set of scans for each image. ViM2 and ViQS uses a stack of multi-resolution convolutions that lets them to capture features at different resolution, resulting in enhancing their performance in dense prediction. Finally, the training of VMamba is based on selective scan [8], while ViM2 (in channel mixing) and ViQS use matrix multiplication of quasi-separable matrices.

## F.8 Difference of ViM, ViM2, and ViQS

The differences of ViM [9] and our methods are the same as their differences with VMamba.

## F.9 How Does Quasi-separable Formulation Use Less Parameters?

One of the most popular approach to make causal models non-causal is to use two separate blocks as forward and backward passes and then consider their summation [37, 9, 38]. This approach, however, results in  $\times 2$  parameters as each block has its own parameters. Our formulation of quasi-separable matrices is an alternative method for this approach that does not need two separate blocks. While the number of parameters in the S6 is the same for both of these forms, quasi-separable form allows to avoid additional convolution and projections for forward and backward passes, resulting in about 40% less parameters than the Forward+Backward method.

## F.10 Experiments on NLP Tasks

The main focus of this study is on the importance of (selective) channel mixing in multi-dimensional data, such as images, videos, and multivariate time series. Accordingly, all the experiments are focused on vision, time series, and speech tasks, and we leave the evaluation of the importance of selective channel mixing on NLP tasks for future work.

# G Experimental Settings and the Details of Models

## G.1 Model Architectures

In this section, we provide the model architectures we used for each task.

Table 7: Settings for Image Classification.

Parameter	ImageNet-1K	sCIFAR
Image size	224 <sup>2</sup>	1024
Dropout	0	0.25
Batch size	1024	50
Training epochs	300	250
Optimizer	AdamW	AdamW
Optimizer momentum	$\beta_1, \beta_2 = 0.9, 0.999$	-
Learning rate	1e-3	0.0045
Weight decay	0.05	0.01
Learning rate schedule	cosine decay	cosine decay
Warmup epochs	10	10
Warmup schedule	linear	linear

**General Architecture Design.** For gated multi-resolution convolutions, we construct features  $F_1, F_2,$  and  $F_3$  with resolution  $\frac{1}{8}, \frac{1}{16},$  and  $\frac{1}{32}$ . We then use depthwise convolutions with kernel sizes of  $k = 3, 5, 7$ . We follow the setting of Mamba for other parameters [8].

We focus on a set of 16 potential scans: (1) Cross-Scan (4 scans:  $C_1, \dots, C_4$ ) [41], (2) Zigzag Scan (8 scans:  $Z_1, \dots, Z_8$ ) [73], and Local Scan (4 scans:  $L_1, \dots, L_4$ ) [64].

**Classification (ImageNet).** For MambaMixer and QSMixer, we follow previous work [13], and match the layers with a ViT-base architecture with 12 layers, a hidden size of 768, an intermediate projection size of 3072, and a patch size of  $16 \times 16$  pixels. For optimization, we follow the training of M2 [13]: we use augmentations such as RandAugment [98] (magnitude = 9, magnitude-std = 0.5, layers = 2), Mixup [99], CutMix [100], Random erasing [101] (rate = 0.25), and AugMix [102]. See Table 7 for additional details.

**Classification (sCIFAR).** The images are represented as the sequences of length 1024 with three channels corresponding to RGB values. Following previous studies [103], we re-scaled and centered the data between  $[-1, 1]$ . We trained the network for 250 epochs with batch size 50 with AdamW optimizer and default hyperparameters. Details are reported in Table 7.

**Object Detection.** In this experiment, we evaluate and compare the performance of ViM2 and ViQS with baselines on object detection using the MSCOCO 2017 dataset [69]. Following the experimental setup of Liu et al. [41], we use the training framework on the mmdetection library [104]. We fine-tune the pre-trained classification models on ImageNet-1K for both 12 and 36 epochs. Again, we use AdamW optimizer with learning rate of 0.0001.

**Semantic Segmentation.** In this experiment, we evaluate the performance of ViM2 and ViQS models on ADE20K dataset [105] and compare them with state-of-the-art baselines. Following Liu et al. [41], we construct a UperHead [106] on top of the pre-trained model. We use crop size of  $512 \times 512$ . While again using AdamW optimizer [107], we set the learning rate as 0.00006, and use a batch size of 16 in fine-tuning.

## H How Do Vanilla MambaMixer and QSMixer Work?

In this section, as a proof of concept, we focus on employing simple MambaMixer and QSMixer for vision, timeseries forecasting and classification, and speech separation tasks.

### H.1 Experiments: SViM2 and SViQS in Image Classification

The results of SViM2 and SViQS are reported in Table 15. SViM2 and SViQS achieve on par performance with many specially designed architectures for vision tasks. These results obtained while these methods are *not* heirarchical and also are depth-wise convolution and attention along the sequence free.

### H.2 Experiments: Video Understanding

In this experiment, to show the applicability of MambaMixer and QSMixer as backbones for a diverse set of vision tasks, we evaluate their performance in temporal action segmentation and temporal action localization tasks on GTEA [108], HACS Segment [109], respectively. To this end, we use the architecture design of ActionFormer [110] and ASFormer [111], but replace the transformer architecture with MambaMixer and QSMixer blocks. We re-use the results of the baselines from Chen et al. [75].

The results are reported in Table 8 and Table 9. Both MambaMixer and QSMixer achieve better results than window attention [112], ViM [9] (i.e., bidirectional Mamba [8]), DBM [75] in both tasks. These results also highlight the importance of channel mixing for multi-dimensional data such as videos.

### H.3 Model: Timeseries MambaMixer (TSM2) and QSMixer (TSQS)

In the next experiment, we evaluate the performance of MambaMixer and QSMixer for time series analysis. To this end, we use simple MambaMixer and QSMixer blocks with layer normalization, called TSM2 and TSQS, respectively. Accordingly, our methods mix and select information across

Table 8: Results of temporal action localization on HACS Segment [109]. The metric is mean Average Precision (mAP) under multiple tIoU thresholds {0.5, 0.75, 0.95}.

Method	Block	mAP@0.5	mAP@0.75	mAP@0.95
ActionFormer [110]	Window Attn [112]	62.62	44.61	12.73
ActionMamba [9]	ViM [9]	63.78	45.45	13.01
ActionMamba [75]	DBM [75]	64.02	45.71	13.34
ActionMambaMixer (ours)	MambaMixer	<b>64.11</b>	<b>45.92</b>	13.39
ActionQSMixer (ours)	QSMixer	64.06	45.83	<b>13.44</b>

Table 9: Results of temporal action segmentation on GTEA [108] dataset. The metrics are accuracy, edit distance [113], and instance-wise F1 under multiple tIoU thresholds {0.1, 0.25, 0.5}.

Method	Block	Acc	Edit	F1@10	F1@25	F1@50
MS-TCN [114]	Dilated Conv, Enc	76.3	79.0	85.8	83.4	69.8
ASFormer [111]	Window Attn [112] Enc-Dec	<b>79.7</b>	84.6	90.1	88.8	79.2
ASFormer [111]	Window Attn [112], Enc-Dec	77.1	81.0	86.2	84.8	77.0
ASFormer [111]	Window Attn [112], Enc	75.4	78.1	82.7	80.5	68.4
ASMamba [9]	ViM [9], Enc	79.3	87.0	90.3	89.0	77.9
ASMamba [75]	DBM [75], Enc	78.4	87.5	91.1	89.8	79.7
ASMambaMixer (ours)	MambaMixer (ours)	78.8	<b>88.0</b>	<b>91.7</b>	<b>90.4</b>	<b>80.1</b>
ASQSMixer (ours)	QSMixer (ours)	78.9	87.8	91.5	90.3	<b>80.0</b>

both time and variates, resulting in selection of both important time stamps and relevant channels for forecasting.

#### H.4 Experiments: TSM2 and TSQS

**Setup.** We perform experiments on 8 publicly available benchmark datasets of real-world multivariate time series, commonly used in studies on long-term forecasting [94, 32, 95]. We compare the performance of TSM2 and TSQS with the state-of-the-art models on multivariate time series forecasting: i.e., SAMFormer [94], simple cross-variate Transformer [94], TSMixer [32], Informer [4], Autoformer [93], FEDFormer [97], Pyraformer [10], and LogTransformer [115]. All time series are segmented with input length  $L = 512$ , prediction horizons  $H \in \{96, 192, 336, 720\}$ , and a stride of 1. Baseline results are reported by either the original paper or Ilbert et al. [94].

**Results.** We compare the MSE results of TSM2 and TSQS with baselines’ in Table 10. TSM2 outperforms the baselines in most cases (18 out of 32 cases as the best model and 8 as the second best model). After TSM2, our TSQS is the second best model with achieving the best results in 8 out of 32 cases and second best in 16 out of 32. The reason for the superior performance of TSM2 and QSMixer is: While some baselines have focused more on cross-time dependencies [4, 97], some others are designed to focus more on cross-variate dependencies [94]. This choice, however, depends on the nature of the dataset. TSM2 and TSQS can learn whether to focus more on cross-variate or cross-time dependencies in a data-driven manner. That is, the dual selection mechanism in MambaMixer and QSMixer not only allows TSM2 and TSQS to capture long-range dependencies but it also uses data-dependent weights, making model more generalizable; while some baselines like TSMixer [32] uses data-independent simple MLPs to fuse information, lacking the selection ability. These results also highlight the importance of selective channel mixing for multivariate time series data.

#### H.5 Experiments: Speech Separation

In this experiment, we evaluate the performance of MambaMixer and QSMixer in speech separation task on WSJ0-2mix dataset [116]. We follow the architecture of DPMamba [117] and replace Mamba with MambaMixer (or QSMixer). Note that, due to the nature of the task and data, here the selective channel mixer is applied on the speech sources after encoding. The results are reported in Table 11 (baseline result are reported by [117]) and show the superior performance of MambaMixer compare to the baselines with the same number of parameters.

Table 10: Performance comparison between our MambaMixer and baselines for multivariate long-term forecasting with different horizons H. Results of baselines are obtained from Ilbert et al. [94]. We display the MSE of methods. Best results are bolded and highlighted in blue, second best are highlighted in gray.

Dataset	H	TSQS (Ours)	TSM2 (Ours)	SAMFormer [2024]	Transformer [2024]	TSMixer [2023]	Informer [2021]	Autoformer [2021]	FEDFormer [2022]	Pyraformer [2021]	LogTransformer [2019]
ETTh1	96	<b>0.374</b>	0.376	0.381	0.509	0.398	0.941	0.435	0.376	0.664	0.878
	192	0.410	<b>0.397</b>	0.409	0.535	0.426	1.007	0.456	0.423	0.790	1.037
	336	0.419	<b>0.416</b>	0.423	0.570	0.435	1.038	0.486	0.444	0.891	1.238
	720	0.426	<b>0.423</b>	0.427	0.601	0.498	1.144	0.515	0.469	0.963	1.135
ETTh2	96	<b>0.255</b>	0.264	0.295	0.396	0.308	1.549	0.332	0.332	0.645	2.116
	192	0.338	<b>0.331</b>	0.340	0.413	0.352	3.792	0.426	0.407	0.788	4.315
	336	0.355	<b>0.347</b>	0.350	0.414	0.360	4.215	0.477	0.400	0.907	1.124
	720	0.398	0.403	<b>0.391</b>	0.424	0.409	3.656	0.453	0.412	0.963	3.188
ETTm1	96	<b>0.319</b>	0.321	0.329	0.384	0.336	0.626	0.510	0.326	0.543	0.600
	192	0.354	<b>0.348</b>	0.353	0.400	0.362	0.725	0.514	0.365	0.557	0.837
	336	0.373	<b>0.370</b>	0.382	0.461	0.391	1.005	0.510	0.392	0.754	1.124
	720	0.419	<b>0.413</b>	0.429	0.463	0.450	1.133	0.527	0.446	0.908	1.153
ETTm2	96	0.176	<b>0.174</b>	0.181	0.200	0.211	0.355	0.205	0.180	0.435	0.768
	192	<b>0.228</b>	0.236	0.233	0.273	0.252	0.595	0.278	0.252	0.730	0.989
	336	0.283	<b>0.279</b>	0.285	0.310	0.303	1.270	0.343	0.324	1.201	1.334
	720	0.397	0.388	<b>0.375</b>	0.426	0.390	3.001	0.414	0.410	3.625	3.048
Electricity	96	0.147	<b>0.144</b>	0.155	0.182	0.173	0.304	0.196	0.186	0.386	0.258
	192	0.159	<b>0.156</b>	0.168	0.202	0.204	0.327	0.211	0.197	0.386	0.266
	336	<b>0.175</b>	0.175	0.183	0.212	0.217	0.333	0.214	0.213	0.378	0.280
	720	<b>0.208</b>	0.213	0.219	0.238	0.242	0.351	0.236	0.233	0.376	0.283
Exchange	96	0.167	0.165	0.161	0.292	0.343	0.847	0.197	<b>0.139</b>	-	0.968
	192	0.241	<b>0.234</b>	0.246	0.372	0.342	1.204	0.300	0.256	-	1.040
	336	0.379	0.384	<b>0.368</b>	0.494	0.484	1.672	0.509	0.426	-	1.659
	720	1.009	<b>0.998</b>	1.003	1.323	1.204	2.478	1.447	1.090	-	1.941
Traffic	96	<b>0.395</b>	0.398	0.407	0.420	0.409	0.733	0.597	0.576	2.085	0.684
	192	0.416	<b>0.409</b>	0.415	0.441	0.637	0.777	0.607	0.610	0.867	0.685
	336	0.423	0.427	<b>0.421</b>	0.501	0.747	0.776	0.623	0.608	0.869	0.734
	720	0.454	<b>0.449</b>	0.456	0.468	0.688	0.827	0.639	0.621	0.881	0.717
Weather	96	<b>0.166</b>	0.174	0.197	0.227	0.214	0.354	0.249	0.238	0.896	0.458
	192	0.221	<b>0.218</b>	0.235	0.256	0.231	0.419	0.325	0.275	0.622	0.658
	336	0.269	<b>0.262</b>	0.276	0.278	0.279	0.583	0.351	0.339	0.739	0.797
	720	<b>0.330</b>	0.337	0.334	0.353	0.343	0.916	0.415	0.389	1.004	0.869
#Best (Second)		8 (16)	18 (8)	4 (8)	0 (0)	0 (0)	0 (0)	0 (0)	1 (1)	0 (0)	0 (0)

## I Additional Experimental Results

### I.1 The Effect of Scanning

We focus on a set of 16 potential scans: (1) Cross-Scan (4 scans:  $C_1, \dots, C_4$ ) [41], (2) Zigzag Scan (8 scans:  $Z_1, \dots, Z_8$ ) [73], and Local Scan (4 scans:  $L_1, \dots, L_4$ ) [64]. We first examine whether using different scans can improve the performance. To this end, we use QSMixer architecture but in each row it uses only the specified scan. Table 12 report the results. Given each set of scans, increasing the variants of a scan can improve the performance but damage the throughput. That is, using only unidirectional-scan (from the set of Cross-Scan [41]) achieves 79.3% but have the throughput of 1039 image/s. Using bi-directional scan or full set of cross-scan, while improving the performance damages the throughput. The similar pattern can be seen for zigzag and local scans. On the other hand, using SoS, not only improve the performance by 0.4%, but it also has the best throughput compared to other cases with similar accuracy. This results, in addition to our ablation study support the significance of SoS.

### I.2 The Effect of Kernel Size

In this experiment, we evaluate the effect of the kernel size of the convolutions on the performance of ViM2 and ViQS. To this end, we use  $k = 3, 5, 7, 9$  and report the performance of these methods on object detection. The main reason of this choice is that, we use these convolutions to improve the multi-resolution view and capturing of local features, which is particularly important for object detection.

The results are reported in Table 13. Results show that  $AP^b$  and  $AP^m$  peak when using kernel sizes 3 and 5, therefore we use these values in our default setting. However, the overall architecture is more robust to the size of the kernel(s).

Table 11: A comparison of MambaMixer and QSMixer with state-of-the-art separation models on WSJ0-2mix [116].

Model	SI-SNRi (dB)	SDRi (dB)	#Params (M)	Stride
Conv-TasNet [118]	15.3	15.6	5.1	8
Sudo rm -rf (B=36) [119]	19.5	n.r.	23.2	10
Wavesplit [120]	22.2	22.3	29	1
TasNet [121]	10.8	11.1	-	20
DPRNN [122]	18.8	19.0	2.6	1
VSUNOS [123]	20.1	20.4	7.5	2
DPTNet [124]	20.2	20.6	2.6	1
Sepformer [125]	22.3	22.4	25.7	8
QDPN [126]	23.6	-	200	8
Mossformer (L) [127]	22.8	-	42.1	8
TD-Conformer-XL [128]	21.2	-	102.7	8
Separate And Diffuse [129]	23.9	-	-	8
Mossformer2 (L) [130]	24.1	-	55.7	8
S4M-tiny [131]	19.4	19.7	1.8	8
S4M [131]	20.5	20.7	3.6	8
DPMamba-S [117]	21.4	21.6	8.1	8
DPMamba-M [117]	22.6	22.7	15.9	8
MambaMixer (ours)	22.7	22.9	15	8
QSMixer (ours)	22.4	22.7	15	8

Table 12: Classification performance using difference scans.

Scan	Throughput (img/s)	Accuracy (%)
Cross-Scan (1)	1189	79.3
Cross-Scan (2)	1166	81.1
Cross-Scan (4)	1129	81.2
Zigzag Scan (1)	1201	79.8
Zigzag Scan (2)	1171	81.3
Zigzag Scan (4)	1108	81.3
Local Scan	1113	81.0
Local + Global Scan	1060	81.3
SoS	1172	81.7

### I.3 The Effect of Resolution on Accuracy and Throughput

We compare the generalizability to inputs of our methods with baselines. Table 14 reports the results. The baseline results are reported by Liu et al. [41]. Both ViM2 and ViQS show more stable results when we increase the resolution. They achieve the best trade-off of throughput and accuracy, compared to the baselines.

Table 13: The effect of kernel sizes on the performance of ViQS and ViM2 in object detection.

Kernel	AP <sup>b</sup>	AP <sup>m</sup>	#Parameters (M)
ViQS			
{3}	47.3	42.4	40
{3, 5}	<b>47.5</b>	<b>42.6</b>	40
{3, 5, 7}	47.4	42.6	40
{3, 5, 7, 9}	47.2	42.1	40
ViM2			
{3}	47.7	42.8	48
{3, 5}	<b>48.1</b>	<b>43.2</b>	48
{3, 5, 7}	47.9	43.0	48
{3, 5, 7, 9}	47.7	42.9	48

Table 14: Comparison of generalizability to inputs with increased spatial resolutions.

Model	Image size	#Param.	FLOPs	Throughput	ImageNet top-1 acc.
ResNet50 [2016]	224 <sup>2</sup>	26	4.1	2988	76.4
	384 <sup>2</sup>	26	12.1	1192	76.5
	512 <sup>2</sup>	26	21.5	705	73.4
	640 <sup>2</sup>	26	33.5	435	69.7
	768 <sup>2</sup>	26	48.3	309	65.3
	1024 <sup>2</sup>	26	85.9	181	52.1
ConvNeXt [2022]	224 <sup>2</sup>	29	4.5	1107	82.0
	384 <sup>2</sup>	29	13.1	405	81.0
	512 <sup>2</sup>	29	23.3	225	78.0
	640 <sup>2</sup>	29	36.5	147	74.3
	768 <sup>2</sup>	29	52.5	103	69.5
	1024 <sup>2</sup>	29	93.3	60	55.4
Deit [2021]	224 <sup>2</sup>	22	4.6	1559	1 80.7
	384 <sup>2</sup>	22	15.5	494	78.9
	512 <sup>2</sup>	22	31.8	256	74.2
	640 <sup>2</sup>	22	58.2	144	68.0
	768 <sup>2</sup>	22	98.7	87	70.0
	1024 <sup>2</sup>	22	243.1	36	46.9
Swin [2021]	224 <sup>2</sup>	28	4.5	1061	81.2
	384 <sup>2</sup>	28	14.5	305	80.7
	512 <sup>2</sup>	28	26.6	168	79.0
	640 <sup>2</sup>	28	45.0	85	76.6
	768 <sup>2</sup>	28	70.7	52	73.1
	1024 <sup>2</sup>	28	152.5	22	61.9
HiViT [2023]	224 <sup>2</sup>	19	4.6	1259	81.9
	384 <sup>2</sup>	19	15.2	392	81.5
	512 <sup>2</sup>	19	30.6	186	79.3
	640 <sup>2</sup>	19	54.8	93	76.0
	768 <sup>2</sup>	19	OOM	OOM	OOM
	1024 <sup>2</sup>	19	OOM	OOM	OOM
VMamba [2024]	224 <sup>2</sup>	31	4.9	1226	82.5
	384 <sup>2</sup>	31	14.3	450	82.5
	512 <sup>2</sup>	31	25.4	272	81.1
	640 <sup>2</sup>	31	39.6	170	79.3
	768 <sup>2</sup>	31	57.1	117	76.1
	1024 <sup>2</sup>	31	101.5	66	62.3
ViQS (ours)	224 <sup>2</sup>	23	4.7	1256	83.8
	384 <sup>2</sup>	23	13.8	468	83.7
	512 <sup>2</sup>	23	24.5	292	82.5
	640 <sup>2</sup>	23	38.2	174	80.4
	768 <sup>2</sup>	23	55	121	78.1
	1024 <sup>2</sup>	23	97.8	67	64.8
ViM2 (ours)	224 <sup>2</sup>	28	5.3	1235	83.8
	384 <sup>2</sup>	28	15.6	461	83.8
	512 <sup>2</sup>	28	27.7	276	82.7
	640 <sup>2</sup>	28	43.1	168	80.4
	768 <sup>2</sup>	28	62	120	78.3
	1024 <sup>2</sup>	28	110.1	67	65.3

#### I.4 Efficiency

We further evaluate the efficiency and scalability of our methods. In the first experiment, we use synthetic data to evaluate the scalability of MambaMixer and QSMixer with respect to the sequence length. Figure 5 shows the results. Both MambaMixer and QSMixer scale smoothly (sub-quadratic) with respect to the length of the sequence. Comparing the quasi-separable formulation with scan shows the significance of our efficient algorithm. That is, using the quasi-separable matrices, instead of scan, we can implement the MambaMixer with fast matrix multiplication of quasi-separable matrices and this figure shows  $\approx 1.8\times$  improvement when using our algorithm.

#### I.5 Full Results of ImageNet-1K

We compare the performance of ViM2 and ViQS with more baselines in Table 15. We additionally reported the results of more efficient Transformers as well as methods that are the combination of convolutional networks with Transformers. Our results show the on par performance of ViM2 and ViQS with state-of-the-art methods, while having better efficiency. Using additional

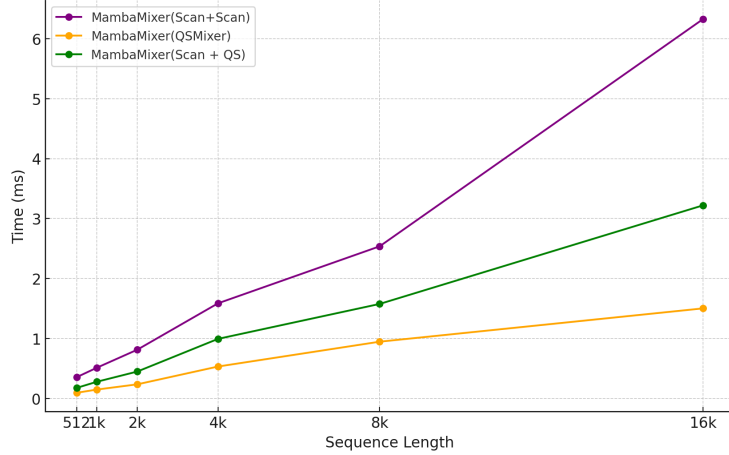


Figure 5: Scaling of MambaMixer and QSMixer with respect to the sequence length.

baselines further validate our claims made in the main paper, and show the significance of the design of ViM2 and ViQS. This is a first step toward using quasi-separable matrices for vision tasks and we believe that the promising results ViM2 and ViQS can motivate future studies to explore more abilities of these methods and further improve their effectiveness of efficiency. Note that, contrary to well-studied methods that are carefully designed to improve efficiency, ViM2 and QSMixer are simple architectures and similar techniques can be added to their architecture in the future work. In fact, the main goal of our experiments is to show the importance of selective channel mixing and present a simple architecture that outperforms its counterparts based on other architectural backbones.

Table 16: Semantic segmentation results on ADE20K using UperNet [67].

Method	Size	mIoU-S	mIoU-M	#Param. (M)	#FLOPs
ResNet-50 [2016]	512 <sup>2</sup>	42.1	42.8	67	953
ResNet-101 [2016]	512 <sup>2</sup>	42.9	44.0	85	1030
DeiT-S + MLN [2021]	512 <sup>2</sup>	43.8	45.1	58	1217
DeiT-B + MLN [2021]	512 <sup>2</sup>	45.5	47.2	144	2007
Swin-T [2021]	512 <sup>2</sup>	44.4	45.8	60	945
Swin-S [2021]	512 <sup>2</sup>	47.6	49.5	81	1039
Swin-B [2021]	512 <sup>2</sup>	48.1	49.7	121	1188
CrossFormer-S [2022]	512 <sup>2</sup>	47.6	48.4	62	980
UniFormer-S [2022]	512 <sup>2</sup>	47.0	48.5	52	955
MPViT-S [2022]	512 <sup>2</sup>	48.3	-	52	943
ConvNeXt-T [2022]	512 <sup>2</sup>	46.0	46.7	60	939
ConvNeXt-S [2022]	512 <sup>2</sup>	48.7	49.6	82	1027
ConvNeXt-B [2022]	512 <sup>2</sup>	49.1	49.9	122	1170
ViT-CoMer-T [2024]	512 <sup>2</sup>	43.0	44.3	38.7	-
ViT-CoMer-S [2024]	512 <sup>2</sup>	46.5	47.7	61.4	-
ViT-CoMer-B [2024]	512 <sup>2</sup>	48.8	49.4	144.7	-
ViM-T [2024]	512 <sup>2</sup>	41.0	-	13	-
ViM-S [2024]	512 <sup>2</sup>	44.9	-	46	-
SiMBA-S [2024]	512 <sup>2</sup>	49.0	49.6	62	-
VMamba-T [2024]	512 <sup>2</sup>	47.3	48.3	55	948
VMamba-S [2024]	512 <sup>2</sup>	49.5	50.5	76	1039
VMamba-B [2024]	512 <sup>2</sup>	50.0	51.3	110	1170
ViQS-T	512 <sup>2</sup>	49.6	50.1	51	918
ViM2-T	512 <sup>2</sup>	48.9	49.9	51	920
ViQS-S	512 <sup>2</sup>	49.7	50.8	68	964
ViM2-S	512 <sup>2</sup>	50.3	51.5	74	1025

Table 17: Object detection and instance segmentation results on COCO dataset.

Method	AP <sup>b</sup>	AP <sup>b</sup> <sub>50</sub>	AP <sup>b</sup> <sub>75</sub>	AP <sup>m</sup>	AP <sup>m</sup> <sub>50</sub>	AP <sup>m</sup> <sub>75</sub>	#Param. (M)
ResNet-50 [2016]	38.2	58.8	41.4	34.7	55.7	37.2	44
ResNet-101 [2016]	38.2	58.8	41.4	34.7	55.7	37.2	63
Swin-T [2021]	42.7	65.2	46.8	39.3	62.2	42.2	48
Swin-S [2021]	44.8	66.6	48.9	40.9	63.2	44.2	69
Swin-B [2021]	46.9	-	-	42.3	-	-	107
QuadTree-B-b0 [2022]	38.8	60.7	42.1	36.5	58.0	39.1	24
QuadTree-B-b1 [2022]	43.5	65.6	47.6	40.1	62.6	43.3	34
QuadTree-B-b2 [2022]	46.7	68.5	51.2	42.4	65.7	45.7	45
MPViT-T [2022]	42.2	64.2	45.8	39.0	61.4	41.8	28
MPViT-XS [2022]	44.2	66.7	48.4	40.4	63.4	43.4	30
MPViT-S [2022]	46.4	68.6	51.2	42.4	65.6	45.7	43
ViT-Adapter-S [2021]	44.7	65.8	48.3	39.9	62.5	42.8	48
ViT-Adapter-B [2021]	47.0	68.2	51.4	41.8	65.1	44.9	102
ConvNeXt-T [2022]	44.2	66.6	48.3	40.1	63.3	42.8	48
ConvNeXt-S [2022]	45.4	67.9	50.0	41.8	65.2	45.1	70
ConvNeXt-B [2022]	47.0	69.4	51.7	42.7	66.3	46.0	108
PVTv2-B2 [2022]	45.3	67.1	49.6	41.2	64.2	44.4	45
PVTv2-B3 [2022]	47.0	68.1	51.7	42.5	65.7	45.7	65
PVTv2-B5 [2022]	47.4	68.6	51.9	42.5	65.7	46.0	102
ViT-CoMer-T [2024]	42.1	62.7	45.3	38.0	60.1	40.5	29
ViT-CoMer-S [2024]	45.8	67.0	49.8	40.5	63.8	43.3	50
ViT-CoMer-B [2024]	47.6	68.9	51.9	41.8	65.9	44.9	129
SiMBA-S [2024]	46.9	68.6	51.7	42.6	65.9	45.8	60
VMamba-T [2024]	46.5	68.5	50.7	42.1	65.5	45.3	42
VMamba-S [2024]	48.2	69.7	52.5	43.0	66.6	46.4	64
VMamba-B [2024]	48.5	69.6	53.0	43.1	67.0	46.4	96
ViQS-T	47.5	69.0	50.9	42.6	65.8	45.7	40
ViM2-T	48.1	69.9	52.8	43.2	66.7	46.6	48
ViQS-S	48.2	69.8	53.0	43.3	66.9	46.7	68
ViM2-S	48.7	69.8	52.8	43.5	66.8	46.9	80

## I.6 Full Results of Semantic Segmentation and Object Detection

We compare the performance of ViM2 and ViQS with additional baselines, including specially designed architectures for dense prediction tasks. Our experiments show the outstanding performance of these methods compared to the baselines. These results further support our conclusion in Section 4.

Table 15: Accuracy comparison across various models on ImageNet-1K.

Method	Size	#Param. (M)	#FLOPs	Top-1	Top-5
ConvNets					
ResNet-50 [2016]	224 <sup>2</sup>	25	4.1	78.3	94.3
ResNet-101 [2016]	224 <sup>2</sup>	45	7.9	80.0	95.0
ResNet-152 [2016]	224 <sup>2</sup>	60	11.6	81.3	95.5
RegNetY-4G [2020]	224 <sup>2</sup>	21	4.0	80.0	-
RegNetY-8G [2020]	224 <sup>2</sup>	39	8.0	81.7	-
RegNetY-16G [2020]	224 <sup>2</sup>	84	16.0	82.9	-
EffNet-B3 [2019]	300 <sup>2</sup>	12	1.8	81.6	-
EffNet-B4 [2019]	380 <sup>2</sup>	19	4.2	82.9	-
RepViT-M1.5 [2024]	224 <sup>2</sup>	14.0	-	82.3	-
RepViT-M2.3 [2024]	224 <sup>2</sup>	22.9	-	83.3	-
Mixer					
Mixer-B/16 [2021]	224 <sup>2</sup>	59	-	76.4	-
Mixer-L/16 [2021]	224 <sup>2</sup>	207	-	71.8	-
ConvMixer-768/32 [2023]	224 <sup>2</sup>	21	-	80.2	-
ConvMixer-1536/20 [2023]	224 <sup>2</sup>	52	-	81.4	-
M2-ViT-b [2023]	224 <sup>2</sup>	45	-	79.5	94.5
Transformers					
ViT-b + Monarch [2023]	224 <sup>2</sup>	33	-	78.9	94.2
ViT-B/16 [2021]	384 <sup>2</sup>	86	17.6	77.9	-
DeiT-S [2021]	224 <sup>2</sup>	22	4.6	79.8	-
DeiT-B [2021]	224 <sup>2</sup>	86	17.5	81.8	-
Swin-T [2021]	224 <sup>2</sup>	29	4.5	81.3	95.5
Swin-S [2021]	224 <sup>2</sup>	50	8.7	83.0	96.2
Swin-B [2021]	224 <sup>2</sup>	88	15.4	83.5	96.5
iFormer-S [2022]	224 <sup>2</sup>	20	4.8	83.4	96.6
iFormer-B [2022]	224 <sup>2</sup>	48.0	9.4	84.6	97.0
Wave-ViT-S [2022]	224 <sup>2</sup>	22.7	4.7	83.9	96.6
Wave-ViT-B [2022]	224 <sup>2</sup>	33.5	7.2	84.8	97.1
CrossFormer-T [2022]	224 <sup>2</sup>	27.8	2.9	81.5	-
CrossFormer-S [2022]	224 <sup>2</sup>	31	4.9	82.5	-
QuadTree-B-b1 [2022]	224 <sup>2</sup>	13.6	2.3	80.0	-
QuadTree-B-b2 [2022]	224 <sup>2</sup>	24	4.5	82.7	-
HorNet-T [2022]	224 <sup>2</sup>	23	4.0	83.0	-
XcIT-T24 [2021]	224 <sup>2</sup>	12.1	2.3	79.4	-
Dual-attention					
DaViT-T [2022]	224 <sup>2</sup>	28.3	4.5	82.8	-
DaViT-S [2022]	224 <sup>2</sup>	49.7	8.8	84.2	-
DaViT-B [2022]	224 <sup>2</sup>	87.9	15.5	84.6	-

Method	Size	#Param. (M)	#FLOPs	Top-1	Top-5
Efficient Transformers					
MobileViT-S [2022]	256 <sup>2</sup>	5.6	2.0	78.4	-
EfficientFormer-L1 [2022]	224 <sup>2</sup>	12.3	1.3	79.2	-
EfficientFormer-L3 [2022]	224 <sup>2</sup>	31.3	3.9	82.4	-
EfficientFormer-L7 [2022]	224 <sup>2</sup>	82	10.2	83.3	-
EfficientMod-S [2024]	224 <sup>2</sup>	12.9	1.4	81.0	-
FastViT-T12 [2023]	256 <sup>2</sup>	6.8	1.4	79.1	-
FastViT-MA36 [2023]	256 <sup>2</sup>	42.7	7.9	83.9	-
FAT-B1 [2023]	224 <sup>2</sup>	7.8	1.2	80.1	-
FAT-B3-ST [2023]	224 <sup>2</sup>	29	4.7	83.0	-
SSMs					
S4ND-ConvNeXt-T [2022]	224 <sup>2</sup>	30	-	82.2	-
S4ND-ViT-B [2022]	224 <sup>2</sup>	89	-	80.4	-
Hyena-ViT-B [2023]	224 <sup>2</sup>	88	-	78.5	93.6
VMamba-T [2024]	224 <sup>2</sup>	22	4.9	82.2	-
VMamba-S [2024]	224 <sup>2</sup>	44	8.7	83.5	-
VMamba-B [2024]	224 <sup>2</sup>	75	15.4	83.2	-
SiMBA-S [2024]	224 <sup>2</sup>	15.3	2.4	81.7	95.9
SiMBA-S (Monarch) [2024]	224 <sup>2</sup>	18.5	3.6	81.1	-
SiMBA-B [2024]	224 <sup>2</sup>	22.8	4.2	83.5	-
SiMBA-B (Monarch) [2024]	224 <sup>2</sup>	26.9	5.5	82.6	-
SiMBA-L [2024]	224 <sup>2</sup>	40	9.0	84.4	-
SiMBA-L (Monarch) [2024]	224 <sup>2</sup>	42	8.7	83.8	-
ViM-T [2024]	224 <sup>2</sup>	7	1.5	76.1	-
LocalViM-T [2024]	224 <sup>2</sup>	8	1.5	75.8	-
ViM-S [2024]	224 <sup>2</sup>	26	5.1	80.5	-
LocalViM-S [2024]	224 <sup>2</sup>	28	4.8	81.0	-
ViM2-MLP (Baseline)	224 <sup>2</sup>	40	9.0	80.1	94.8
ViM2-T (ours)	224 <sup>2</sup>	13.2	2.1	81.9	95.9
ViQS-T (ours)	224 <sup>2</sup>	10.1	1.9	81.7	95.8
ViM2-S (ours)	224 <sup>2</sup>	28	5.3	83.8	96.6
ViQS-S (ours)	224 <sup>2</sup>	23	4.7	83.8	96.5
ViM2-B (ours)	224 <sup>2</sup>	74	17.9	85.0	97.1
ViQS-B (ours)	224 <sup>2</sup>	45	9.0	84.9	97.0
ViM2-L (ours)	224 <sup>2</sup>	122	23.2	85.5	97.3